World Electric Vehicle Journal

MDPI

Article

A Novel Model Chain for Analysing the Performance of Vehicle Integrated Photovoltaic (VIPV) Systems

Hamid Samadi [1,*], Guido Ala [1], Miguel Centeno Brito [2], Marzia Traverso [3], Silvia Licciardi [1], Pietro Romano [1] and Fabio Viola [1]

[1] Department of Engineering, University of Palermo, 90128 Palermo, Italy
[2] Institute of Dom Luiz (IDL), Faculty of Sciences, University of Lisbon, 1749-016 Lisbon, Portugal
[3] Institute of Sustainability in Civil Engineering, RWTH Aachen University, 52062 Aachen, Germany
* Correspondence: hamid.samadi@unipa.it

Abstract

This study proposes a novel framework for analyzing Vehicle-Integrated Photovoltaic (VIPV) systems, integrating optical, thermal, and electrical models. The model modifies existing fixed PV methodologies for VIPV applications to assess received irradiance, PV module temperature, and energy production, and is available as an open-source MATLAB tool (VIPVLIB) enabling simulations via a smartphone. A key innovation is the integration of meteorological data and real-time driving, dynamically updating vehicle position and orientation every second. Different time resolutions were explored to balance accuracy and computational efficiency for optical model, while the thermal model, enhanced by vehicle speed, wind effects, and thermal inertia, improved temperature and power predictions. Validation on a minibus operating within the University of Palermo campus confirmed the applicability of the proposed framework. The roof received 45–47% of total annual irradiation, and the total yearly energy yield reached about 4.3 MWh/Year for crystalline-silicon, 3.7 MWh/Year for CdTe, and 3.1 MWh/Year for CIGS, with the roof alone producing up to 2.1 MWh/Year (c-Si). Under hourly operation, the generated solar energy was sufficient to fully meet daily demand from April to August, while during continuous operation it supplied up to 60% of total consumption. The corresponding CO_2-emission reduction ranged from about 3.5 ton/Year for internal-combustion vehicles to around 2 ton/Year for electric ones. The framework provides a structured, data-driven approach for VIPV analysis, capable of simulating dynamic optical, thermal, and electrical behaviors under actual driving conditions. Its modular architecture ensures both immediate applicability and long-term adaptability, serving as a solid foundation for advanced VIPV design, fleet-scale optimization, and sustainability-oriented policy assessment.

Keywords: vehicle integrated photovoltaic; sustainable transportation; VIPV simulation; solar powered vehicles

Academic Editor: Michael Fowler

Received: 17 September 2025
Revised: 27 October 2025
Accepted: 9 November 2025
Published: 13 November 2025

Citation: Samadi, H.; Ala, G.; Brito, M.C.; Traverso, M.; Licciardi, S.; Romano, P.; Viola, F. A Novel Model Chain for Analysing the Performance of Vehicle Integrated Photovoltaic (VIPV) Systems. *World Electr. Veh. J.* **2025**, *16*, 619. https://doi.org/10.3390/wevj16110619

1. Introduction

The increasing demands for environmentally sustainable and efficient transportation systems have intensified the need for innovative solutions [1], including the use of renewable energy and clean fuel alternatives [2,3]. A notable advancement in this field may be the integration of photovoltaic (PV) systems into vehicles, known as Vehicle-Integrated Photovoltaics (VIPV) [4]. VIPV involves using vehicle surfaces, such as the roof, back, and sides, to harness sunlight [5]. These surfaces can generate solar energy, whether the

vehicle is stationary or moving [6]. This energy can then supplement or even replace traditional fuel sources, helping to reduce greenhouse gas emissions and reduce reliance on conventional fuels [7]. As the world focuses more on achieving carbon-neutral transportation, VIPV has emerged as a possible interesting innovation with the potential to provide major environmental benefits [8,9]. Moreover, in recent years, advancements in solar cell efficiency, lightweight materials, and advanced energy management systems have significantly enhanced the feasibility of VIPV systems [10–12].

However, despite these advances, the practical implementation of VIPV remains challenging. Moving vehicles experience dynamic conditions, including variations in orientation, speed, and shading [13], while the usable area and safe integration of PV modules on curved or partially shaded vehicle surfaces also limit performance. Therefore, a detailed understanding of how solar radiation interacts with vehicle geometry and driving conditions is essential to achieve reliable system performance predictions.

Many experimental investigations into VIPV systems have been conducted. For example, Peibst et al. [14] analyzed a truck equipped with amorphous silicon PV modules along a 36 km route in Hanover, Germany. Their study examined solar radiation received on the roof, sides, and back of the vehicle under both stationary and moving conditions, showing that the roof consistently received the highest irradiance and that orientation and shading strongly influenced performance. Similarly, Ota et al. [15] investigated solar radiation on a vehicle travelling a 15 km route in Miyazaki, Japan. This study highlighted that geographic location, weather conditions, and seasonal variations significantly affect irradiance levels, confirming the difficulty of predicting VIPV performance under dynamic conditions. Building on these efforts, Wetzel et al. [16] analyzed a van equipped with PV modules over a 21 km route in Hanover, considering different urban environments such as narrow streets, wide roads, and open highways, and found that building shading and road geometry had a major impact on energy capture. Together, these works confirmed the high sensitivity of VIPV performance to environmental and operational factors but also showed that results are highly case-specific, making it difficult to generalize findings or design universal assessment methods.

Experimental investigations into VIPV systems have provided valuable insights into their performance under diverse operating scenarios. While these experimental findings are valuable, they also highlight the challenges associated with physical testing [17]. Prototype development and measurement campaigns are costly and time-consuming, and the diversity of driving and weather conditions makes it difficult to compare results across studies. However, simulation-based approach may provide a scalable and flexible way for studying VIPV systems in a pre-prototyping phase, so reducing previous listed uncertainties, and bridging the gap between experimental observations and real-world applications [18–26].

Kutter et al. [24] investigated the integration of PV systems into the roofs of commercial trucks and vans in Europe. Their study used hourly solar data to estimate annual solar energy generation for different vehicle types, such as parcel delivery vans, rural delivery trucks, and long-haul trucks. However, this approach only considered the horizontal roof surface and ignored shading and side-surface contributions, thus limiting the accuracy of real-world predictions. Expanding on this, Kim et al. [23], analyzed the potential for solar energy generation on high-speed trains in South Korea. They used a dynamic model to calculate solar irradiance on the roofs of moving trains and incorporated shadow effects from nearby objects. This method relied on Geographic Information Systems (GIS) data and included a Digital Surface Model (DSM) with a resolution of 3 m to improve accuracy. The calculations were performed at a high temporal resolution, with solar irradiation estimated for each minute. Similarly, Oh et al. [22] studied solar buses in Seoul, South Korea, using high-resolution GIS data to calculate solar power generation, and considering

the specific location of each bus and the surrounding environment, including road networks, topography, and building heights. Similarly, their calculations also used a high temporal resolution, performing estimations every minute to accurately model solar irradiance and energy generation along each bus route.

In addition to solar irradiance, the temperature of PV modules significantly affects their efficiency, as higher temperatures generally reduce performance [27–30]. Researchers have used different methods to calculate module temperatures [31,32]. For example, the Nominal Operating Cell Temperature (NOCT) [33] and Faiman [34] models are widely used for stationary PV systems. However, these models do not account for the thermal inertia of fast-moving PV systems. To address this, Patel et al. [35] proposed averaging temperature variations over periods of 1000 to 1500 s to account for the thermal inertia in moving PV systems.

Beyond temperature considerations, some studies have focused on developing accurate models for PV performance under dynamic conditions. Abdelhamid et al. [25] developed an optimized model for on-board PV systems in plug-in electric vehicles, which integrates both electrical and thermal effects under varying operational conditions. Their approach used a single-diode model (SDM) to calculate key performance indicators such as voltage, current, and power. They applied a four-parameter framework that incorporated curve-fitting techniques to estimate essential factors such as light-generated current, saturation current, diode ideality factor, and series resistance. In another related study, Mallon et al. [36] investigated the integration of on-board PV modules in heavy-duty electric vehicles, focusing on an electric bus to evaluate energy generation under different configurations. The study employed an electrical model based on SDM to assess how power output varied with changes in temperature and solar radiation. This approach included a peak power temperature coefficient to capture the sensitivity of PV performance to temperature fluctuations, complemented by a thermal model based on NOCT model to estimate operating temperatures under varying environmental conditions, including solar irradiance and ambient air temperature.

Unlike many other research areas, there is no widely recognized and standardized methodology for simulating VIPV systems. Although numerous methodologies have been proposed [22–26], selecting the right one for a given study remains a significant challenge. This paper aims to address this challenge by proposing an integrated, open-source model chain that organizes the simulation process for VIPV systems. The proposed framework offers both accuracy and flexibility, ensuring that it can be adapted to various case studies. This approach directly responds to the need for reproducible, dynamic VIPV modeling that links environmental, operational, and technological variables.

The framework consists of three parts, each designed to model critical aspects of a VIPV system:

- Optical Model analyzes how sunlight interacts with the vehicle's surface, considering factors such as shading and the effects of the vehicle's body curvature.
- Thermal Model examines the temperature variations in PV modules due to environmental conditions and heat dissipation, as temperature significantly impacts PV efficiency.
- Electrical Model simulates the electrical behavior of the PV system, including energy generation and power output.

For each of these parts, the most appropriate methodologies have been carefully chosen to build a robust and reliable simulation framework. Moreover, the proposed framework is designed to be flexible and modular, allowing each component to be adapted, replaced, or upgraded with alternative or more advanced models depending on the application, available data, or specific research objectives. To simulate the VIPV system under actual driving conditions, we collected real-world driving data through a smartphone equipped

with MATLAB Mobile. The data includes essential parameters such as vehicle speed, GPS coordinates, and direction. These parameters were processed in MATLAB to simulate the performance of the VIPV system in real-time. This approach allows us to develop a simulation-based framework using real data.

To experimentally validate the proposed methodology, a case study was conducted using a minibus operating within the University of Palermo (UNIPA) campus. The minibus was chosen because of its frequent use for passenger transport and consistent operational patterns. By studying this vehicle in a controlled environment, we were able to collect reliable data and evaluate the performance of the VIPV system under real-world conditions. Additionally, to simulate the energy produced by the VIPV system, we considered the vehicle's energy consumption across different operational scenarios. This comparison enabled us to assess the feasibility and potential benefits of integrating VIPV systems into vehicles. Furthermore, we explored the sustainability implications of integrating VIPV systems into both electric vehicles (EVs) and internal combustion engine (ICE) vehicles, highlighting the potential of VIPV to reduce emissions and support cleaner mobility. This represents a first step toward a future comprehensive life-cycle assessment of VIPV applications.

2. Methodology

Figure 1 shows a schematic of the proposed approach. Step 1 involves collecting real-time driving data from MATLAB Mobile (Version 9.9) (vehicle speed, position, and direction) together with meteorological and geographic parameters from the TMY dataset. Step 2 applies the optical model to compute the irradiance on each vehicle surface using these dynamic inputs. Step 3 estimates the PV module temperature at every second through the thermal model, and Step 4 refines this estimation by incorporating thermal inertia to capture transient effects. Step 5 combines the optical and thermal outputs within the electrical model to determine instantaneous power and cumulative energy generation. This sequential workflow ensures consistent data exchange among all components, accurately representing the dynamic behavior of a moving vehicle.

The optical model developed in this study builds upon methodologies proposed by Perez et al. [37] and King et al. [38], which estimates the diffuse and direct irradiance received by surfaces based on weather data and geographic location. These methods are typically applied to stationary PV systems and calculate irradiance on surfaces with defined tilt and orientation over a specified time range. To address this, our methodology accounts for vehicle movement, as the position of the vehicle relative to the sun will continuously change. These variations mean that, depending on the time ($t = [t_1, \ldots, t_n]$) and position ($\begin{bmatrix} Latitude \\ Longitude \end{bmatrix} = \begin{bmatrix} Lat_1 & Lat_n \\ Lon_1, \ldots, & Lon_n \end{bmatrix}$), each solar cell integrated into different surfaces of the vehicle will experience varying azimuth (γ). Consequently, the irradiance received by each surface will vary every second.

Real-time driving data was collected using the MATLAB Mobile application, which utilizes smartphone sensors to capture detailed information on the vehicle's geographic position, speed, and direction of travel. Data points were recorded at one-second intervals, resulting in a high-resolution temporal dataset. The vehicle's path is thus modeled as a sequence of discrete positions with continuously updated orientation. This dynamic input allows the optical model to compute irradiance for each surface, roof, back, and sides, at every time step, reflecting the actual conditions experienced by the vehicle during motion. Furthermore, to understand how the choice of temporal resolution affects the accuracy of optical model, simulations were run at different time intervals: 1, 2, 3, 4, 5, and 10 min. These results were compared against the one-second baseline to evaluate the potential errors introduced by coarser time steps. This analysis highlights the importance

of high-resolution modeling, especially for mobile PV systems where rapid changes in environmental exposure are frequent.

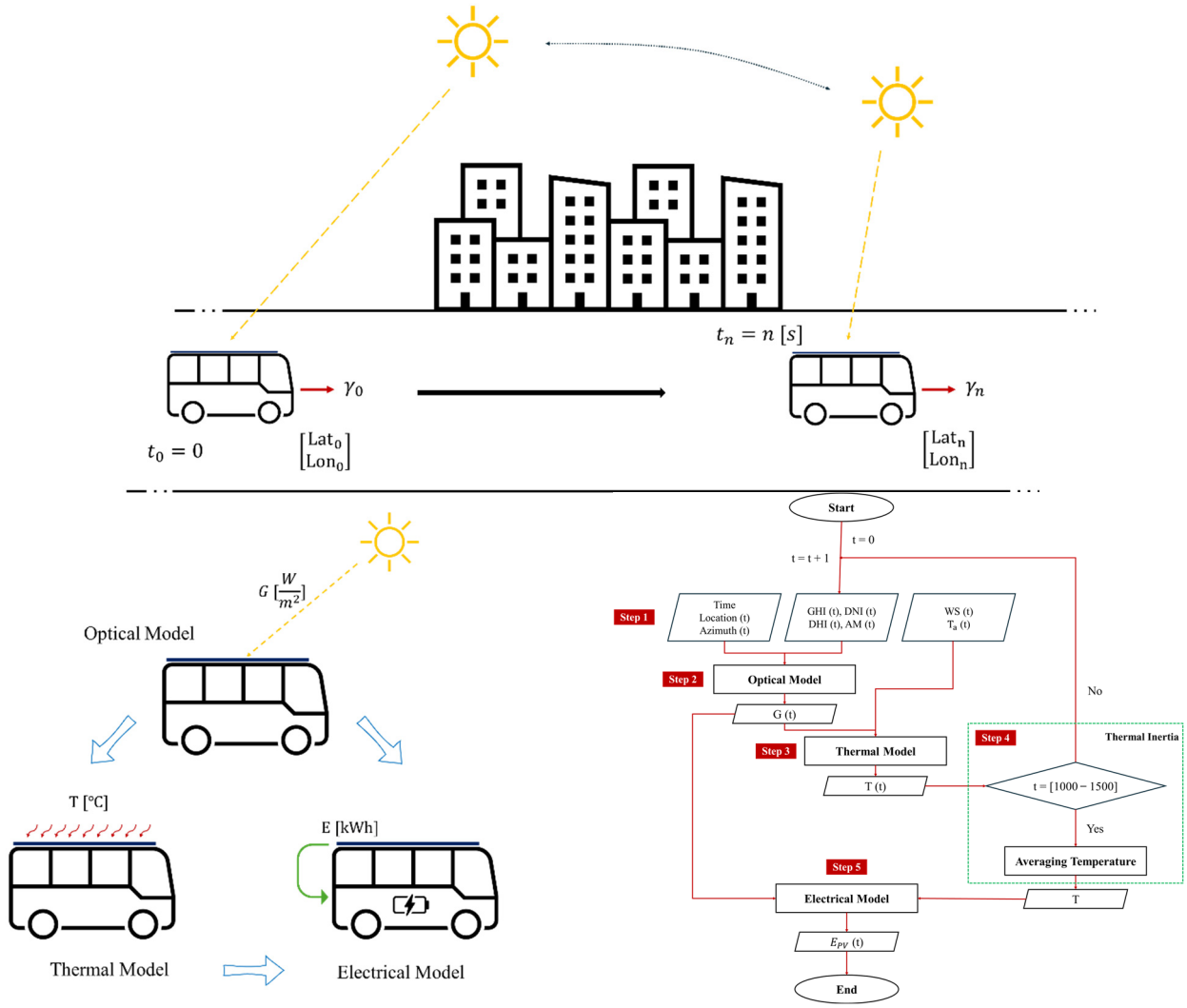

Figure 1. The proposed model chain for investigating the performance of VIPV systems.

To provide the necessary meteorological data for simulation, Typical Meteorological Year (TMY) files were used. These datasets compile representative hourly weather conditions over a full year for specific geographic locations. For this study, TMY data for Palermo was obtained from the Photovoltaic Geographical Information System (PVGIS) portal [39]. The TMY datasets include essential parameters such as Direct Normal Irradiance (DNI), Diffuse Horizontal Irradiance (DHI), ambient temperature (T_a), and wind speed (WS). Since the optical and thermal models operate on a per-second basis, linear interpolation was applied to the TMY data to transform it into a higher temporal resolution. The use of TMY data was preferred because it provides a statistically consistent representation of long-term meteorological conditions and is widely adopted in PV system modeling, ensuring comparability with other studies. However, TMY data represent averaged weather patterns and do not capture short-term fluctuations or extreme conditions that may occur in real driving environments. This simplification can introduce some uncertainty in second-by-second VIPV simulations, where transient irradiance or temperature spikes could slightly alter results. Future developments may address this limitation by coupling the model with high-frequency meteorological data or real-time measurements collected through onboard sensors.

Thermal behavior was analyzed using both the Nominal Operating Cell Temperature (NOCT) model and the Faiman model. These approaches estimate the PV module temperature based on external environmental conditions and module-specific properties. To account for thermal inertia, which becomes significant in fast-moving PV applications, the method proposed by Patel et al. [35] was incorporated. This ensures that transient thermal effects, such as delayed temperature response due to rapid changes in environmental conditions or vehicle motion, are appropriately considered. The integration of optical and thermal models forms the foundation for estimating electrical energy generation. To perform this estimation, the single-diode model was employed. This model calculates the power output of the PV system at each second, using inputs from the optical and thermal simulations. The results are then aggregated to evaluate performance across various timeframes, including daily, monthly, and annual periods.

Given that photovoltaic technologies differ in characteristics such as conversion efficiency, temperature coefficient, and spectral response, their performance can vary significantly under dynamic operating conditions [40]. To explore this, a comparative analysis was conducted on three widely used PV technologies: crystalline silicon (c-Si), copper indium gallium selenide (CIGS), and cadmium telluride (CdTe). Each technology was evaluated in the context of VIPV to understand how it responds to changes in irradiance, temperature, and orientation over time.

Finally, to complement the energy generation analysis, a vehicle model was developed to estimate energy consumption during motion. This model is essential for comparing the amount of energy generated by the VIPV system with the actual demand of the vehicle under different driving scenarios. All the models proposed in this study, the optical, thermal, electrical, and vehicle consumption models, are discussed individually and in greater detail in the following sections.

2.1. Optical Model

Solar radiation has three main components: direct, diffuse, and reflected ones. In this study, the reflection component wasn't considered; therefore, the total irradiance incident on the solar cells integrated into the vehicle can be expressed as in Equation (1) [41]:

$$G_t = G_b + G_d \tag{1}$$

Although direct solar irradiance (G_b) travels in a straight path to the PV module, diffuse solar irradiance (G_d) consists of rays scattered by atmospheric particles, approaching the solar module from different directions. Another important factor considered in the optical model is the shading, which directly affects the amount of incoming irradiance available to the photovoltaic system. The impact of shading varies significantly across different environments due to factors such as the density of trees, buildings, and other obstructions along the paths. When shading is not severe, its effect can be approximated using a constant shading loss factor, as defined in Equation (2) [7,26,36]:

$$G_{b\ (Shading)} = \eta_{Shading} \cdot G_b \tag{2}$$

where $G_{b\ (Shading)}$ represents the direct irradiance accounting for shading effects, allowing for a simplified yet effective assessment of the shading's influence on the overall performance of the VIPV system. The impact of the shading on the diffuse irradiance could be modelled considering a sky view factor approach [42] but, except in severe shading conditions, it may be neglected: this is the choice adopted in the proposed approach. The curvature of the vehicle body also has an impact on the harvesting of solar energy. Ota et al. [43] introduced geometric parameters and proposed a metric known as the Curve

Correction Factor (CF) to account for this curvature during the simulation process. This factor allows for a more accurate estimation of the PV system's performance by compensating for the effects of the vehicle's curved surface on solar energy capture. By incorporating the CF, the model can better reflect the real-world performance of vehicle-integrated photovoltaic systems, ensuring a more reliable analysis of their efficiency. By using CF, finally, the total received irradiance on the vehicle body, accounting for both shading effects and CF, is expressed as follows:

$$G = CF \cdot \left(G_{b\ (Shading)} + G_d\right) \tag{3}$$

By using Equation (4), the amount of direct irradiance on a surface can be calculated [25]:

$$G_b = DNI \cdot \cos\ (AOI) \tag{4}$$

where DNI stands for Direct Normal Irradiance and AOI stands for Angle of Incidence. DNI is the direct component of the irradiance received per unit area by a surface that is always oriented perpendicular (normal) to the sun's rays coming directly from the sun's current position in the sky. The AOI is the angle between the incoming solar rays and the normal to the surface receiving the radiation. The Angle of Incidence (AOI) is calculated using the following equation [38]:

$$AOI = \cos^{-1}\left[\cos\ (\beta) \cdot \cos\ (\theta_Z) + \sin\ (\beta) \cdot \sin\ (\theta_Z) \cdot \cos\ (\gamma_S - \gamma)\right] \tag{5}$$

In this context, β represents the tilt angle of the PV surface relative to the horizontal plane, γ denotes the azimuth angle of the PV surface (the angle between the projection of the normal to the surface and a reference direction such as north), θ_Z is the solar zenith angle (the angle between the sun's rays and the vertical direction), and γ_S is the solar azimuth angle (the angle between the projection of the sun's rays on the horizontal plane and the north direction). The angle of incidence, along with other relevant solar angles, is depicted in Figure 2.

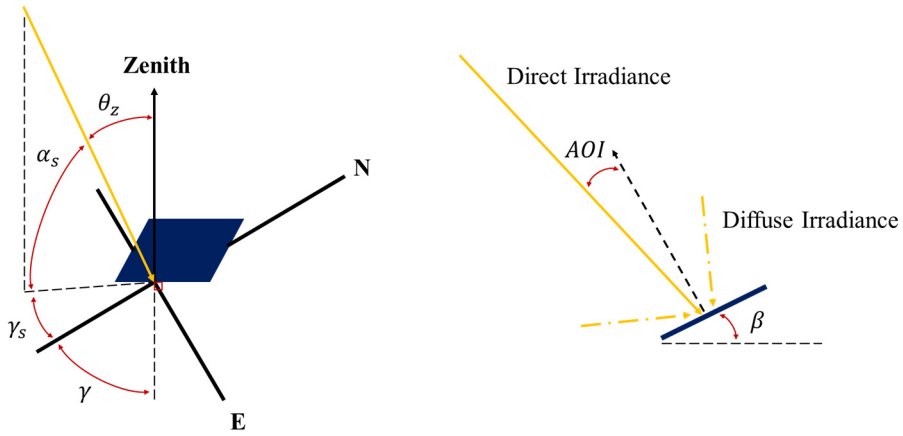

Figure 2. Illustration of different solar angles.

Based on the method proposed by Perez et al. [37], the diffuse irradiance received on a tilted surface (G_d) can be calculated as follows:

$$G_d = DHI \cdot \left[\frac{(1 - F_1) \cdot (1 + \cos\ \beta)}{2} + F_1 \cdot \frac{A}{B} + F_2 \cdot \sin\beta\right] \tag{6}$$

$$A = \max(0, \cos AOI)\ ,\ \ B = \max(0.087, \cos\theta_Z) \tag{7}$$

where F_1 and F_2 are coefficients that express the degree of circumsolar and horizon/zenith anisotropy, respectively. These coefficients vary as functions of sky conditions and can be calculated as follows:

$$F_1 = F_{11} + F_{12} \cdot \Delta + F_{13} \cdot \theta_Z \quad (8)$$

$$F_2 = F_{21} + F_{22} \cdot \Delta + F_{23} \cdot \theta_Z \quad (9)$$

It should be noted that F_{11}, F_{12}, F_{13} and F_{21}, F_{22}, F_{23} are Perez et al. [37] model coefficients, which were calculated based on the sky's clearness (ε):

$$\varepsilon = \frac{DHI + DNI}{DHI + \kappa \cdot {\theta_Z}^3} \cdot \frac{1}{1 + \kappa \cdot {\theta_Z}^3} \quad (10)$$

where κ is a constant equal to 1.041. Based on the obtained value of ε and its range, Perez et al. [37] calculated the corresponding coefficients. Additionally, by using extraterrestrial normal irradiance (E_a) and Air Mass (AM), the sky's brightness (Δ) can be determined as follows:

$$\Delta = \frac{DHI \cdot AM}{E_a} \quad (11)$$

The air mass can be calculated as follows [44]:

$$AM = \frac{1}{\cos(\alpha_S) + 0.50572 \cdot (6.07995 + (90 - \alpha_S))^{-1.6364}} \quad (12)$$

where α_S is the solar elevation angle, the angle between the sun's rays and the horizontal plane, which indicates how high the sun is in the sky.

$$\alpha_S = 90 - \theta_Z \quad (13)$$

Additionally, the extraterrestrial normal irradiance (E_a) is calculated using the following equation:

$$E_a = E_{sc} \cdot \left(\frac{R_{av}}{R}\right)^2 \quad (14)$$

$$\left(\frac{R_{av}}{R}\right)^2 = 1.00011 + 0.034221 \cdot \cos(b) + \frac{0.00128}{\sin(b)} + 0.000719 \cdot \cos(2b) + 0.000077 \cdot \sin(2b) \quad (15)$$

$$b = 2\pi \cdot \frac{doy}{365} \quad (16)$$

where E_{sc} solar constant (1367 W/m^2) represents the average solar radiation received outside the Earth's atmosphere on a surface perpendicular to the sun's rays, doy is the day of the year, R_{av} is the average distance from the Earth to the sun, and R is the actual distance from the Earth to the sun on a given day.

VIPVLIB

PVLIB toolbox in MATLAB [45] provides a set of functions for simulating PV system performance. Some functions available in the PVLIB library are based on methodologies similar to those proposed in the previous section. For instance, the *pvl_getaoi* function in PVLIB calculates the angle of incidence (AOI) using the methodology developed by King et al. [38] and it requires inputs such as γ, γ_S, θ_Z, and β. Parameters such as extraterrestrial normal irradiance (E_a) can be calculated either through analytical expressions (Equations (14)–(16)) or using built-in PVLIB functions such as *pvl_extraradiation* and *pvl_date2doy* to determine E_a and doy. Although PVLIB was originally developed for fixed PV installations, its functions were adapted and integrated into an open-source model

chain developed in this study to account for vehicle dynamics. Figure 3 illustrates the structure and data flow of the optical model, where selected PVLIB functions are combined with real driving and geographical data to compute irradiance on vehicle surfaces in motion. This open-source framework, referred to as "VIPVLIB," includes an optical model based on adapted PVLIB functions, along with thermal and electrical models developed following the methodology proposed in this work. The complete model chain has been made available to support further research in the field of VIPV systems. The thermal and electrical models will be described in detail in the following sections.

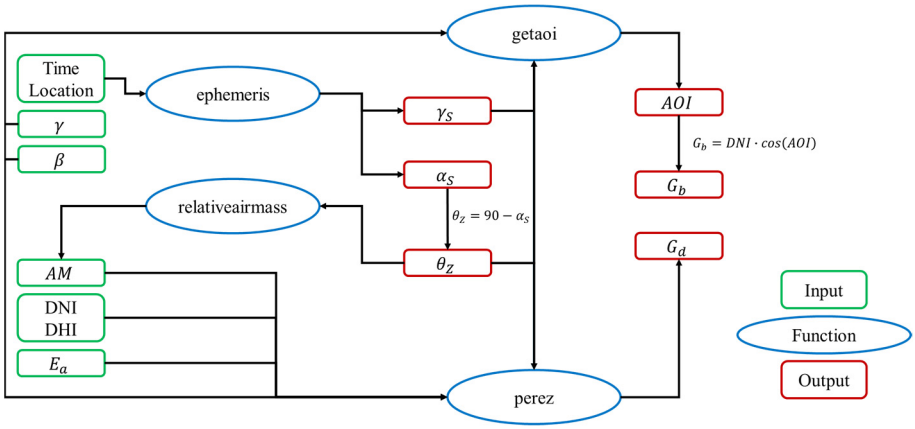

Figure 3. Flowchart of the Optical Model Process Using PVLIB Functions.

2.2. Thermal Model

The thermal model refers to the calculation of the temperature of the PV module (T_{module}) by utilizing meteorological data, the vehicle's velocity, and the solar irradiance obtained from the optical model. As already underlined, NOCT and Faiman methods have been used. The NOCT method provides an estimate of the PV module temperature under specific reference conditions: 800 W/m^2 irradiance, 20 °C ambient temperature, and 1 m/s wind speed. This method is useful for standardizing temperature predictions across different PV technologies and is as follows [33]:

$$T_{module} = T_a + \frac{G_t}{800} \cdot (NOCT - 20) \tag{17}$$

where T_a represents the air temperature. In this work, the NOCT is considered to be 48 [°C]. The Faiman method uses a heat balance equation to model the thermal behavior of the PV cells, considering factors such as air temperature (T_a) °C, wind speed m/s, and the specific thermal properties of the PV module. By using Equation (18), T_{module} can be calculated through the Faiman method [34]:

$$T_{module} = T_a + \frac{G_t}{U_0 + U_1 \cdot WS} \tag{18}$$

where U_0 represents the constant heat transfer component W/m^{2}K, U_1 represents the convective heat transfer component W/m^{3}sK, and WS represents the wind speed m/s. When the vehicle is in motion, the wind speed is determined based on its instantaneous speed. When the vehicle is parked, the ambient wind speed is used. Since wind speed data from TMY is recorded at a height of 10 m above ground, it is adjusted to the roof height using the following equation [46]:

$$WS_{Roof} = WS_{TMY} \cdot \left(\frac{h_{Roof}}{10^{0.2}} \right) \tag{19}$$

Therefore, as discussed in [46], when the vehicle is stopped (speed = 0), the wind speed was adjusted based on the height of the minibus roof to simulate natural airflow. It should be noted that the temperature of the PV modules was first obtained every second using the two mentioned methods. Then, following the approach proposed by Patel et al. [35], the second-by-second temperature data were averaged over intervals of 1000 to 1500 s and used in the electrical model instead of directly using the instantaneous values. This averaging range was chosen because Patel et al. [35] demonstrated that beyond approximately 1000–1500 s, the thermal parameters of PV modules reach steady convergence, indicating that this period represents the characteristic thermal time constant of a moving PV system. Averaging over this interval effectively filters short-term fluctuations while preserving the real thermal response of the modules under dynamic conditions.

2.3. Electrical Model

To calculate the amount of P_{PV}, generated power from the PV modules, this work proposes an electrical model incorporating previous results, including G_t and T_{module}, as follows [36,47]:

$$P_{PV} = \eta_{PV} \cdot \eta_{Co} \cdot A_{PV} \cdot G \cdot \left(1 + k \cdot \left(T_{module} - T_{ref}\right)\right) \quad (20)$$

$$A_{PV} = \alpha \cdot A_{Vehicle} \quad (21)$$

The value of the temperature coefficient (k) depends on the type of solar cell used. A_{PV} refers to the PV coverage area m^2, while α denotes the percentage of the vehicle's surface area covered by PV modules. In this study, the values of efficiency of the power converter (η_{Co}) and reference temperature (T_{ref}) were set to 96% and 25 °C respectively, following the work of [22,23,36]. By calculating the generated power, we can obtain comparable data to investigate and analyze the potential integration of different PV modules into the minibus. This approach enables a systematic evaluation of the effectiveness and efficiency of PV cell applications in automotive contexts.

2.4. Vehicle Model

The vehicle model was developed to estimate the power demand and total energy consumption of the system. It assumes that the driver closely adheres to the reference speed profile provided by the drive cycle. Based on Newton's second law of motion, the total road load is computed as the sum of various forces acting on the vehicle, including the inertial force $\vec{F_i}$ (due to vehicle acceleration a_V), the gravitational force $\vec{F_S}$ from road gradients, rolling resistance $\vec{F_r}$, and aerodynamic drag $\vec{F_a}$, as shown in the following equation [36,48]:

$$\vec{F_t} = \vec{F_i} + \vec{F_s} + \vec{F_r} + \vec{F_a} \quad (22)$$

Figure 4 shows a schematic representation of the vehicle model, and the forces considered. Where M is the total mass kg, g gravitational acceleration m/s^2, ρ is the air density kg/m^3, α_r is road inclination, c_{rr} is rolling resistance coefficient, c_d is the air drag coefficient, A_f is the frontal area m^2, and V is the vehicle speed m/s.

The total power P_{tot} (in W) and total energy consumption E_{tot} (in Wh) are computed using the following equations [48].

$$P_{tot} = F_t \cdot V;\ E_{tot} = \int P_{tot} dt \quad (23)$$

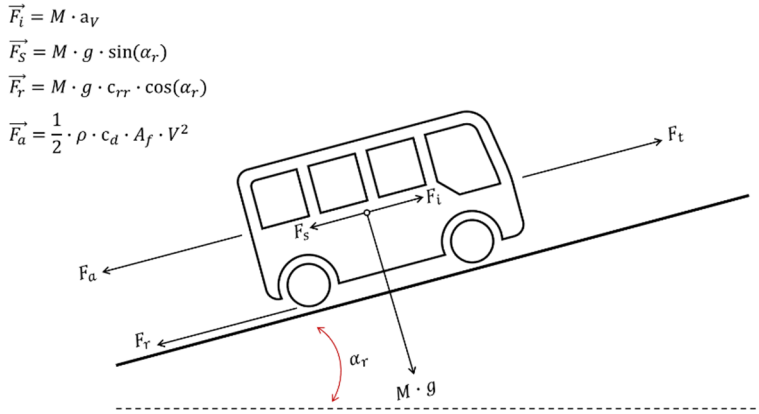

Figure 4. Vehicle model diagram.

3. Case Study

A practical vehicle was selected to apply the proposed methodology based on its frequent usage and operational characteristics. An electric minibus, commonly used within the UNIPA campus, was chosen for this study. This vehicle plays a key role in transporting numerous people around the campus and between departments. Its regular operation in a real-world environment provides an excellent opportunity to investigate the performance of a VIPV system under typical usage conditions, offering valuable data for assessing its efficiency and practical applicability. The vehicle used in this study was the Karsan e-Jest minibus, and its general dimensions are provided in Table 1.

Table 1. Dimensions of the Karsan e-Jest minibus in this study [48,49].

	Considered Dimensions [mm]
Length	5854
Width	2055
Height	2800

These dimensions have been extracted from the vehicle's official catalogue [48,49]. It is important to note that, in this study, we assumed that PV modules cannot fully cover the entire surface area of the minibus. Several factors contribute to this limitation, including the curvature of the vehicle's surfaces, the presence of windows, air conditioning ducts, and other structural features that impede complete coverage. Table 2 details the percentage of the surface area covered by PV modules for different sections of the minibus, as considered in this study. These coverage percentages are based on realistic assessments of usable surface areas that can accommodate PV cells.

Table 2. PV coverage for different surfaces of the minibus.

Surfaces	**PV Coverage [%]**
Top	60
Back	70
Right	40
Left	50

This study also explores different PV technologies to investigate VIPV performance. The specifications of these solar cells are detailed in Table 3.

Table 3. Specifications of the PV modules [50,51].

PV Module	Efficiency [%]	k [%/°C]	U_0 [W/m^2°C]	U_1 [W/m^3°C]
c-Si	21.6	− 0.47	30.02	6.28
CIGS	15.1	− 0.45	22.19	4.09
CdTe	18.6	− 0.34	23.37	5.44

Table 3 provides key parameters such as the cell efficiency (η_{PV}), temperature coefficient (k, in %/°C), etc, which are critical for accurately modeling the thermal and electrical behavior of the PV modules. Moreover, Table 4 presents the required parameters for vehicle modeling [48].

Table 4. Vehicle model parameters.

Parameter	Variable	Value
Vehicle Mass [kg]	M_V	5000
Aerodynamic Drag Coefficient	c_d	0.36
Rolling Resistance Coefficient	c_{rr}	0.011
Air Density [kg/m^3]	ρ	1.202

It should be noted that a 95% drive system efficiency and a constant base power of 2 kW, which accounts for the energy consumption of auxiliary systems, were added to the total power calculation [48].

Vehicle Motion

The movement and orientation of the minibus were tracked using MATLAB Mobile, which utilizes the sensors of a smartphone to gather critical data, including location, speed, and azimuth. This approach facilitated the collection of key inputs essential for the proposed methodology. The location and speed data were recorded at one-second intervals, offering a detailed representation of the minibus's trajectory over a complete trip. In particular, location data, as depicted in Figure 5, illustrates the vehicle's path during its operational cycle. The route included five bus stops, which played a key role in assessing the movement pattern and enhancing the model's precision.

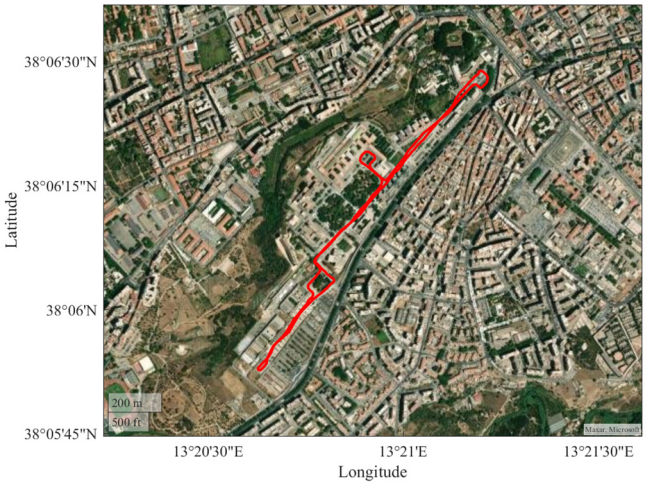

Figure 5. The pathway of the minibus across the University of Palermo (UNIPA) campus (Source: MATLAB R 2023 b).

The ability to capture and utilize such detailed data enhances the robustness of the proposed approach, allowing for a comprehensive analysis of the VIPV system's perfor-

mance under realistic operating conditions. The speed profile of the minibus along the mentioned pathway is shown in Figure 6. As illustrated, the complete drive cycle was 20 min (1200 s). This figure provides a detailed view of the speed fluctuations throughout the cycle, reflecting typical operational conditions.

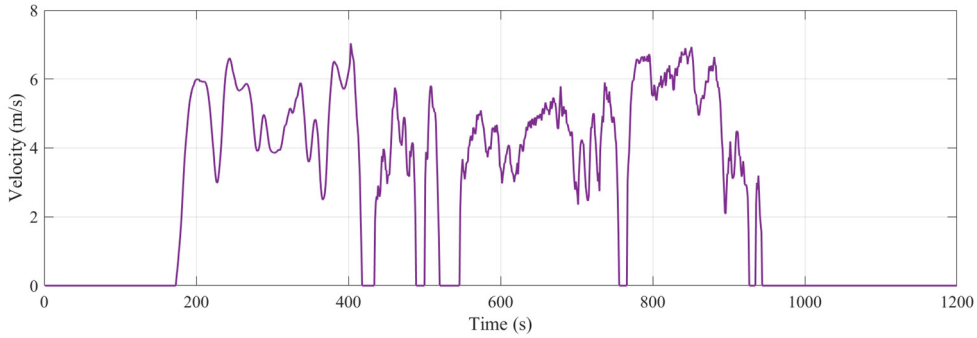

Figure 6. The drive cycle of the minibus.

Understanding speed variations and operational patterns is essential for accurately modeling the minibus and estimating its energy consumption. To explore these aspects, different scenarios were considered. The minibus's operation was based on a drive cycle of 20 min, with the working hours set from 8:00 to 15:00. Under these conditions, the minibus could either operate continuously or run only once per hour. Depending on the operational pattern, this results in the vehicle completing between 7 and 21 trips within the defined working hours.

During the data collection process, the number of passengers onboard the minibus was also recorded, as shown in Figure 7. This information provided key insights into the passenger dynamics across different trips. Two scenarios were developed to examine how the number of passengers affects energy consumption:

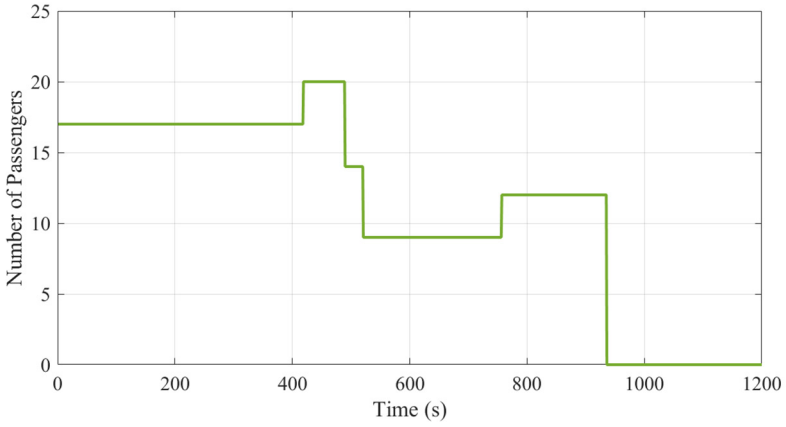

Figure 7. The variations in passenger mass during the trip.

1. Full Capacity: In this scenario, the minibus operates with a constant number of passengers, assuming full capacity of 22 passengers for the entire trip duration.
2. Variable Passenger Count: The number of passengers changes dynamically at each stop, reflecting real-world boarding and alighting patterns (as illustrated in Figure 7).

The average weight of each passenger was 70 kg, which contributed to the vehicle's total load.

Although Figures 6 and 7 present one representative cycle for clarity, multiple trips were recorded under typical operating conditions during different times of the day. The

selected dataset was verified to be consistent with the average behavior of the minibus and is therefore considered representative for modeling purposes and for extrapolation to yearly operation.

The collection of azimuth data resulted in a total of 63,401 values, reflecting the vehicle's directional changes at a high frequency of at least 50 measurements per second. The azimuth data was averaged for each second. This approach preserved the essential directional variations of the minibus while significantly reducing the dataset to a manageable size. The resulting averaged azimuth (Az) values are shown in Figure 8, providing a clear representation of the vehicle's orientation throughout its operational cycle.

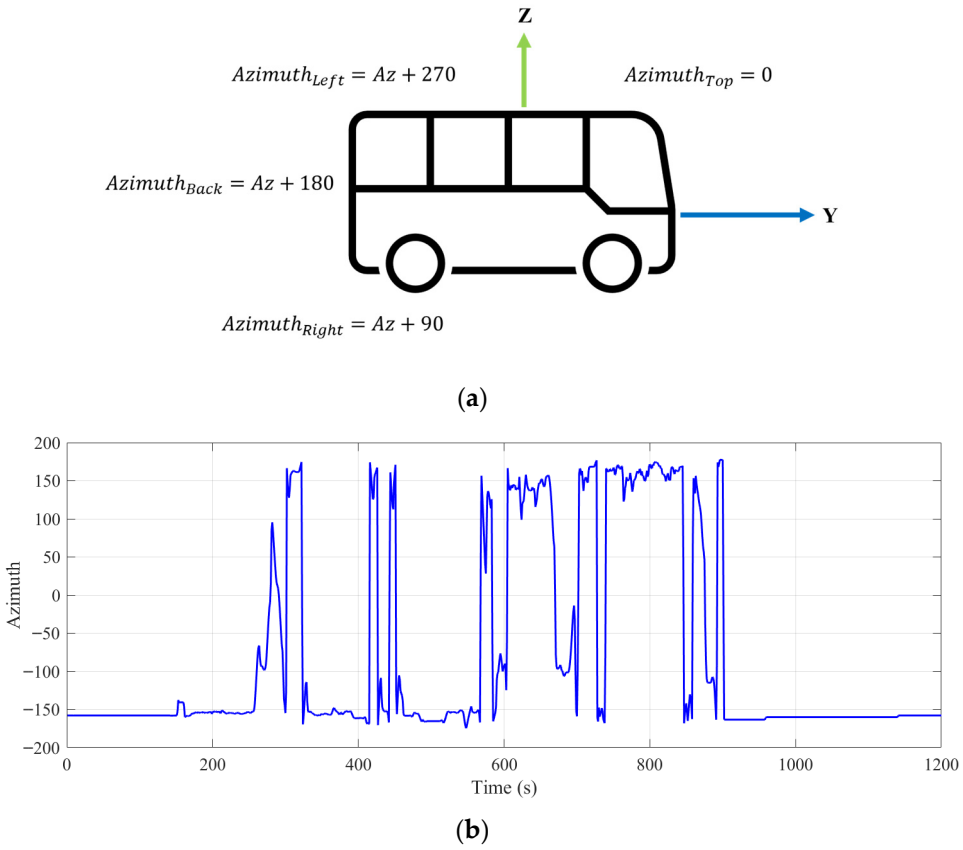

Figure 8. (**a**) The coordinates and (**b**) the azimuth during the minibus trip.

This processed azimuth data is pivotal for subsequent analyses, particularly in calculating solar angles within the optical model. The synchronization and averaging processes also align the azimuth data with other collected variables, providing a robust and coherent dataset for further modeling and analysis.

4. Results and Discussion

The discussion in this section is organized into three main parts. The first part focuses on analyzing the performance of the VIPV system, with a detailed examination of the results obtained from the optical, thermal, and electrical models. In the second part, based on the output of the electrical model and various defined operating scenarios, the vehicle's energy consumption is compared with the energy generated by the VIPV system. Finally, the third part discusses the environmental impact by comparing emissions across different vehicle types, highlighting the potential benefits of integrating VIPV systems.

4.1. Analysis of VIPV System Performance

4.1.1. Optical Model

As mentioned earlier, data collection was conducted on 11 April between 12:00 and 12:20. Accordingly, the simulation was first performed for the optical model using this specific time interval. The results of the optical model, showing the irradiance distribution across different parts of the vehicle, are presented in Figure 9.

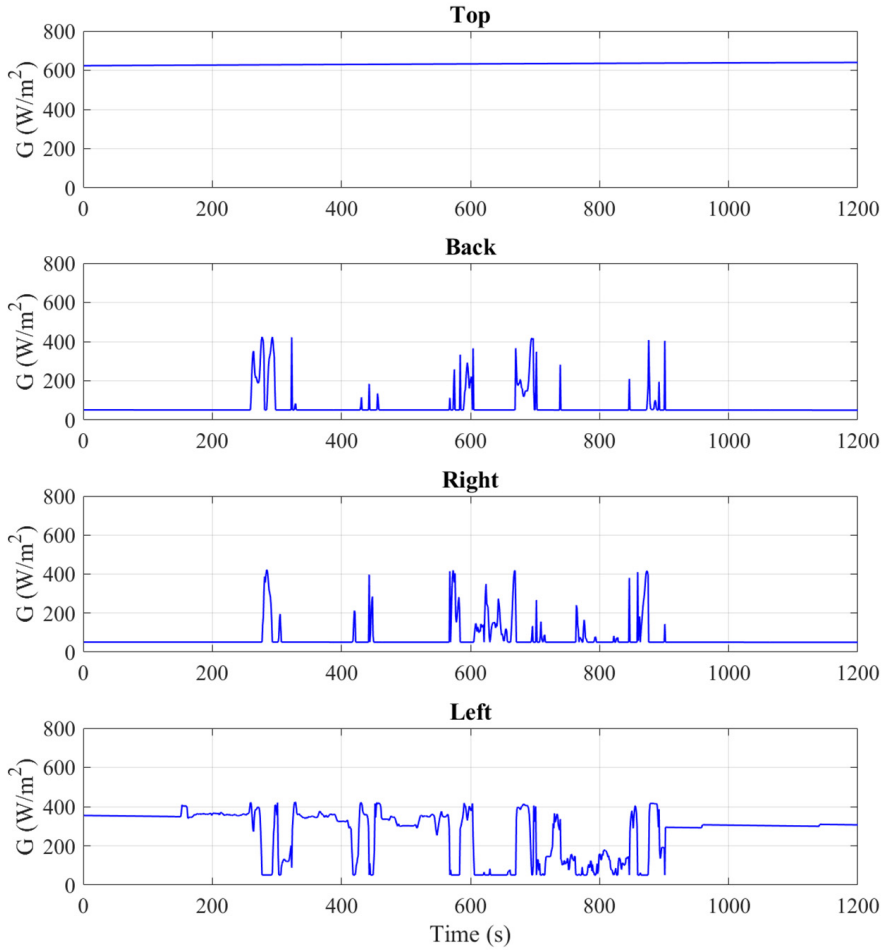

Figure 9. The received irradiance by different sections of the minibus on 11 April, from 12:00 to 12:20.

The analysis reveals that the top surface (roof) of the minibus generally receives higher irradiance compared to its other sides. However, this difference is influenced by seasonal variations and other environmental factors. To investigate these variations in more detail, a continuous operating scenario was simulated in which the vehicle runs from 08:00 to 15:00, with the drive cycle repeated throughout this period. Figure 10 presents the monthly solar irradiation received by different sections of the minibus, along with the percentage contribution of each surface to the total solar irradiation.

Figure 10 illustrates the monthly distribution of solar irradiation received by each surface of the minibus and how it varies due to seasonal changes, the sun's position, and the angle of incidence. The top surface consistently captures the largest portion of solar energy throughout the year, confirming its primary role in the total irradiation collected by the vehicle. As shown, this surface reaches its highest contribution during June and July, accounting for about 46–47% of the total irradiation, while during the winter months (December and January), it decreases to around 38–39%. By contrast, the side and back surfaces absorb lower but still significant shares. The right side shows its maximum contribution during summer (around 25%) and maintains relatively stable levels across

most months. The left side, on the other hand, becomes more dominant during the winter months, reaching about 22–23% of the total irradiation, which can be attributed to lower solar elevation angles that favor lateral surfaces under certain orientations. The back surface contributes less overall, typically ranging between 10–13%, with slightly higher values in spring months.

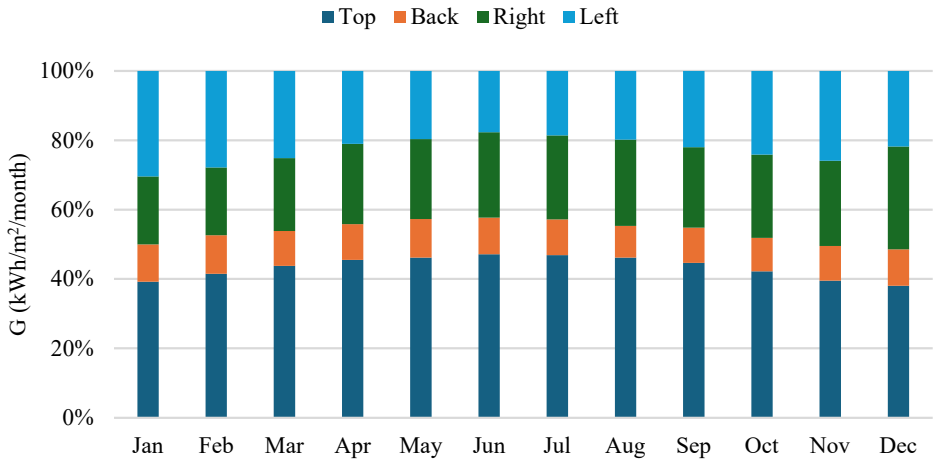

Figure 10. Fraction of monthly irradiation for the different sections of the minibus.

This pattern also reflects the effect of vehicle orientation and sun angles along the route. Differences between the right and left sides result from variations in the minibus's heading during its circular pathway. Although the route is circular, the vehicle does not spend equal time on outbound and return legs because of stop locations and dwell times. The observed seasonal and directional fluctuations highlight the importance of using high temporal resolution in simulations to accurately represent dynamic variations in irradiation. In this study, simulations were performed at a per-second resolution to capture rapid changes in solar angles, vehicle heading, and location. In the following section, we further examine how reducing this temporal resolution can influence the estimation of annual solar irradiation received by each surface, and we evaluate the associated trade-offs in simulation accuracy, data volume, computational demand, and overall model performance.

To evaluate the influence of temporal resolution on the estimation of solar irradiation for VIPV, the simulation was repeated at progressively coarser time steps (1, 2, 3, 4, 5, and 10 min) and compared with the baseline 1-s resolution. Figure 11 illustrates how temporal downsampling affects both the spatial geometry of the vehicle path and the resulting irradiation estimates for different surfaces. The path plots show that as the time step increases, the number of recorded points along the route drastically decreases, removing small heading fluctuations and geometric details. This loss of directional information strongly affects surfaces with orientation-dependent exposure. The bar chart of annual irradiation shows that while the top surface remains almost unaffected, the side and back surfaces become increasingly inconsistent. The absolute percentage error plot confirms this: the top surface remains below 1% error, while the back surface shows extreme sensitivity (errors exceeding 100%), and the right and left sides reach up to 35–40% error at some resolutions.

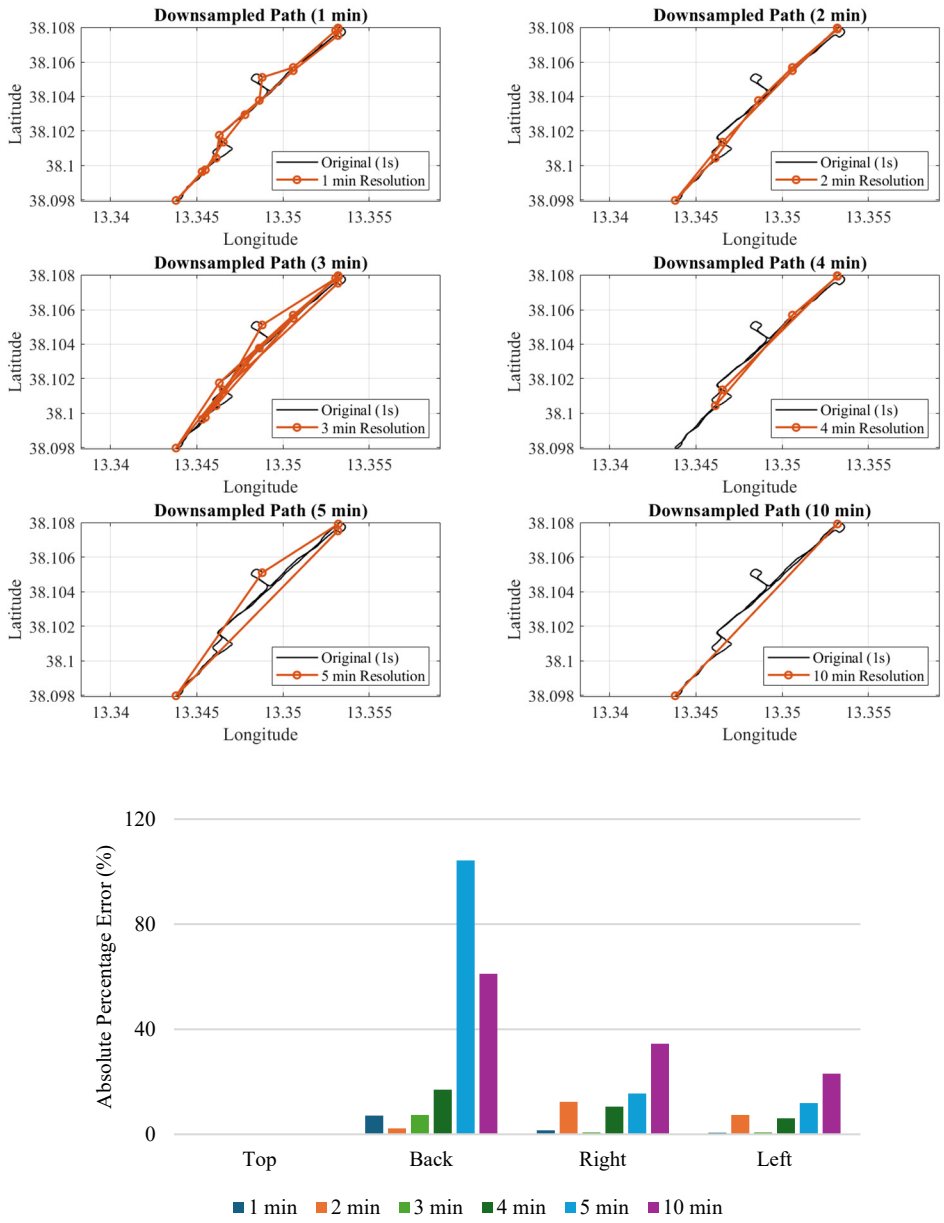

Figure 11. Effect of temporal resolution on path geometry and annual irradiation estimation for each vehicle surface.

4.1.2. Thermal Model

After determining the irradiance using the optical model, the temperature of the integrated PV modules on different surfaces of the minibus can be calculated through the thermal model. Figure 12 presents the moving average temperature for each cycle from 08:00 to 15:00 on 11 April.

As shown in Figure 12, in the NOCT model, the PV technology does not significantly affect the results. In contrast, the Faiman model incorporates different coefficients for various solar cell types, leading to varied temperature outcomes for each type. A key advantage of the Faiman model in the VIPV context is its consideration of wind speed. By including wind speed as a factor, the Faiman model offers a more accurate estimation of PV module temperatures under real-world operating conditions, making it potentially more suitable for this application.

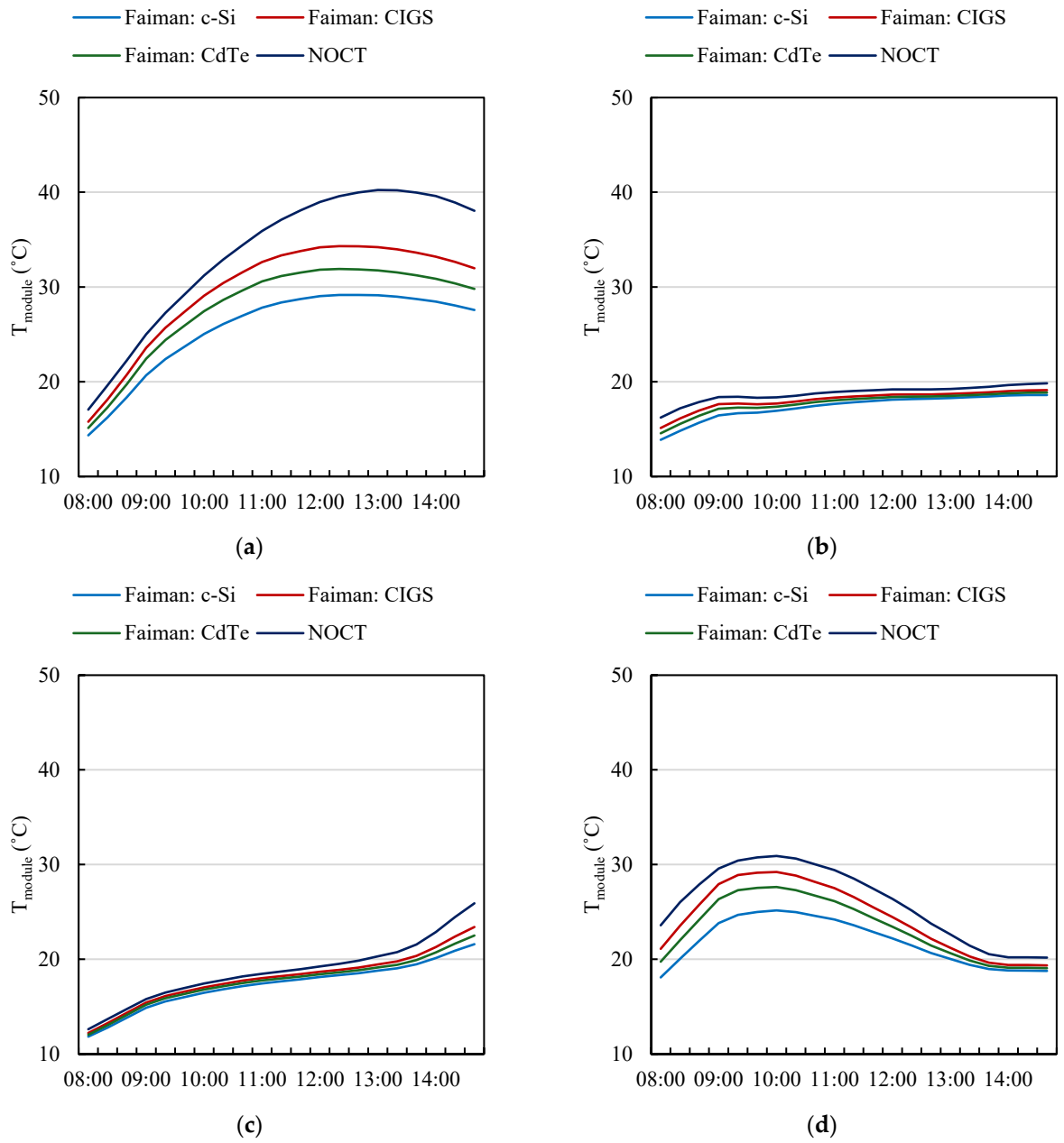

Figure 12. Calculated module temperatures using the Faiman and NOCT models for various PV module types which integrated into (**a**) top, (**b**) back, (**c**) right, and (**d**) left surfaces on 11 April, from 08:00 to 15:00.

4.1.3. Electrical Model

In general, lower PV module temperatures lead to higher efficiency and greater power output, as reduced thermal losses improve the overall performance of solar cells. Based on the results obtained from the thermal model, the Faiman model was selected to calculate PV module temperatures for use in the electrical model. Figure 13 presents the total yearly electrical energy generated by different types of solar modules installed on various surfaces of the minibus.

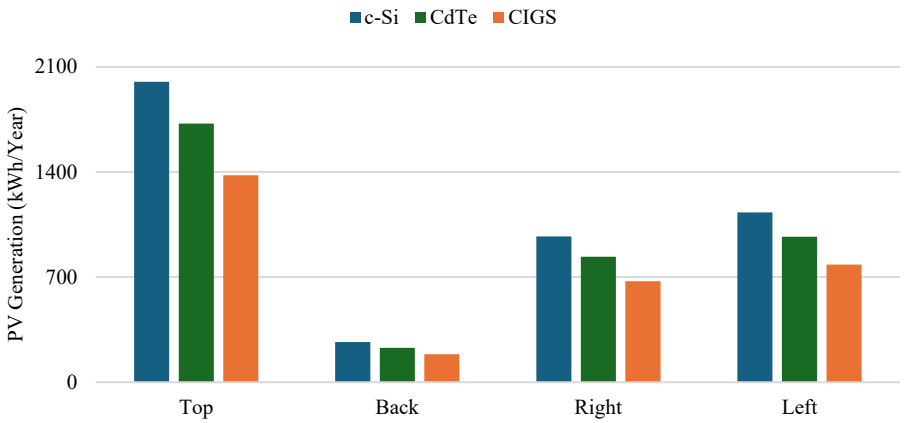

Figure 13. Yearly electrical energy generated by different types of solar modules integrated into various surfaces of the minibus, based on results from Faiman model.

The crystalline silicon (c-Si) photovoltaic modules produced more energy due to their higher efficiency. Hence, Figure 14 illustrates the distribution of daily energy generated across different months by the c-Si modules integrated into various sections of the minibus. These results provide valuable insights into how seasonal variations and environmental conditions, such as temperature and solar irradiance, impact energy production throughout the year.

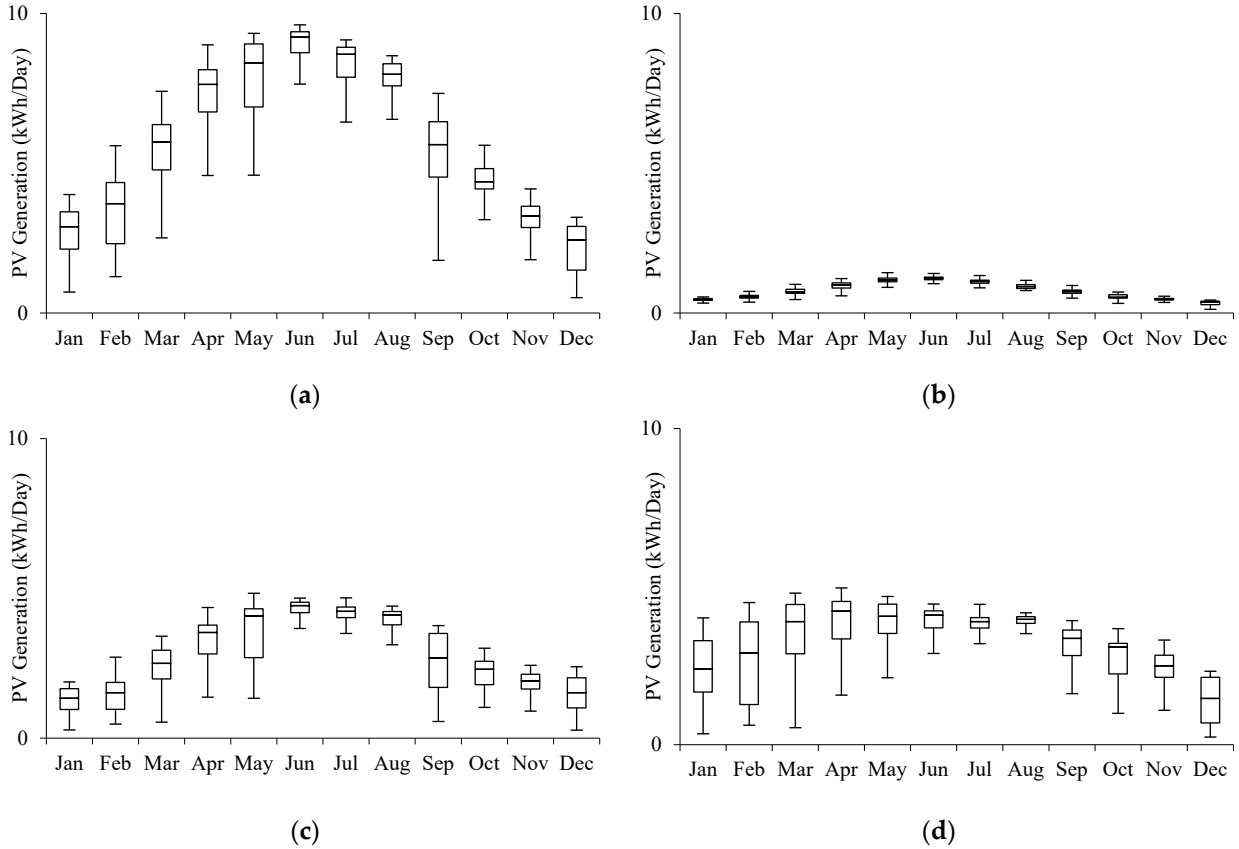

Figure 14. Distribution of daily PV generation across different months using crystalline silicon (c-Si) photovoltaic modules integrated on the (**a**) top, (**b**) back, (**c**) right, and (**d**) left sides of the minibus.

4.2. Analysis of Different Operating Scenarios on Energy Consumption

Based on the vehicle model, the results obtained for the power and energy requirements of the minibus are presented in Figure 15. These results correspond to two different

scenarios regarding the number of passengers. In the first scenario, the minibus is at full capacity with 22 passengers, while in the second scenario, the number of passengers varies based on data collected during the trip.

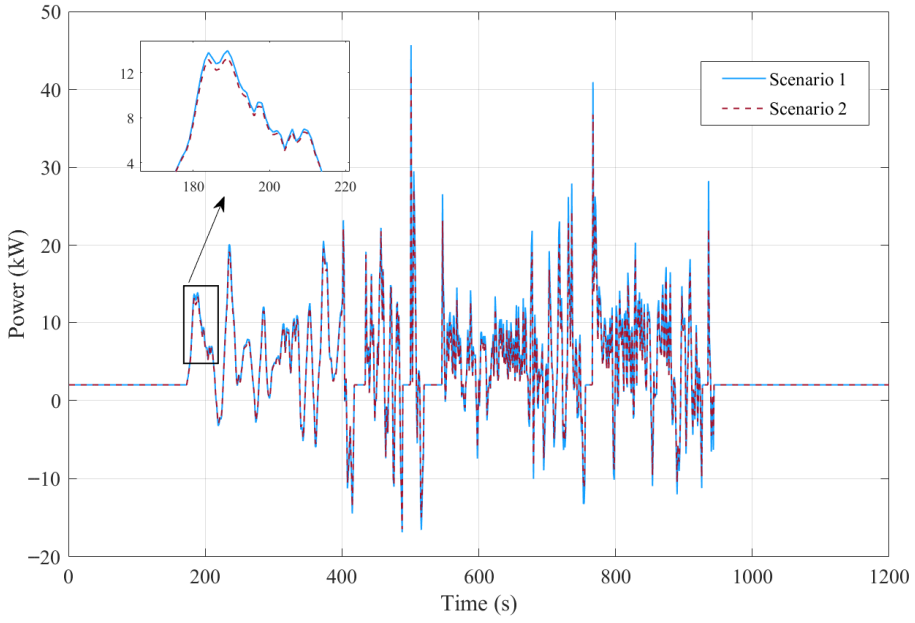

(**a**)

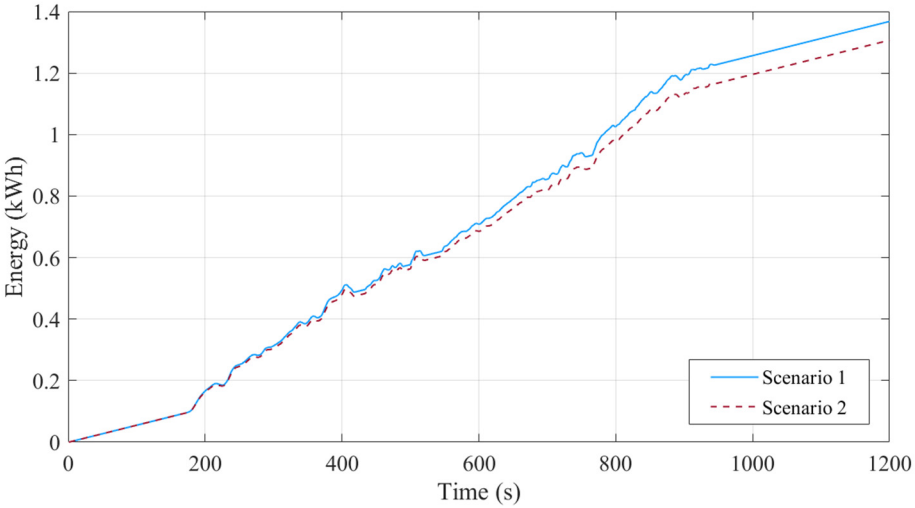

(**b**)

Figure 15. Estimated (**a**) power requirements and (**b**) energy requirements of the minibus in both defined scenarios.

The required energy for the minibus was calculated as about 1.4 kWh for the first scenario (full capacity) and 1.3 kWh for the second scenario (variable passengers). These results show that the impact of the passenger load is not very relevant to the energy requirements of the minibus, with a slight reduction in energy demand when the number of passengers is lower, as observed in the second scenario.

In the following, we also compared different operational conditions for the minibus. This comparison was made to investigate the impact of these different working conditions on energy generation. In the first case, we assumed the minibus operates continuously without any gaps during work hours, from 08:00 to 15:00. In the second scenario, we considered the minibus operating once per hour. When parked, the minibus is always in

the sunshine. The number of cycles the minibus completes during the day directly impacts energy consumption. In the continuous operation scenario, the minibus (Full capacity scenario) undergoes 21 cycles per day, while in the hourly operation scenario, only 7 cycles occur. As shown, this results in an energy consumption of approximately 29 kWh/day in the continuous scenario and approximately 10 kWh/day in the hourly scenario, assuming the bus is full during these cycles. The number of days in each month that the VIPV system can power the minibus is determined based on the energy generated and consumed in each scenario. Figure 16 presents this data as a percentage, illustrating the monthly contribution of the VIPV system to fulfilling the vehicle's energy requirements throughout the year.

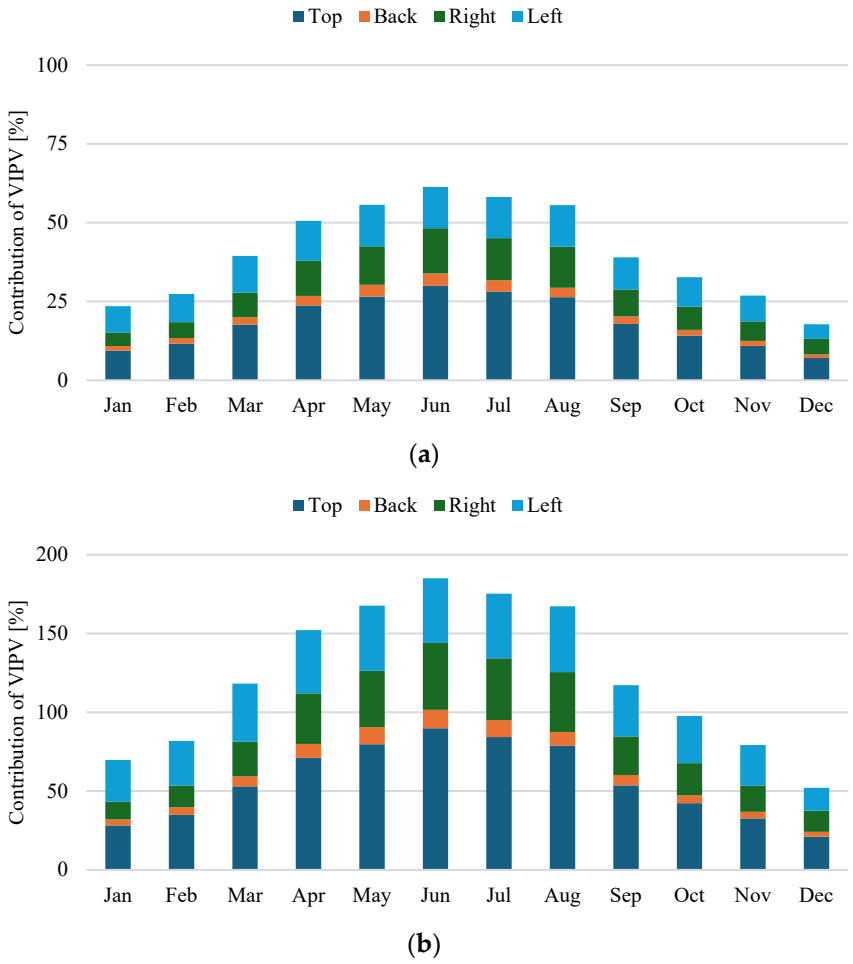

Figure 16. The monthly contribution of the VIPV system to the energy requirements of the minibus under two scenarios: (**a**) continuous operation and (**b**) hourly operation.

As shown in this figure, in the hourly scenario, the energy generated by the VIPV system exceeds the energy consumption from April to August. This is due to the lower energy requirements in the hourly scenario compared to the continuous scenario, also the vehicle is parked during gap times in areas without shading, leading to higher solar irradiance and increased energy generation.

4.3. Analysis of CO_2 Emissions by Vehicle Type

Although EVs are increasingly promoted in Europe and other regions, internal combustion engine (ICE) vehicles are still widely used in many areas. Previous sections of this study focused on the case study of an electric minibus. In this section, the analysis of a minibus powered by an internal combustion engine is also presented to assess how CO_2 emissions vary when the VIPV concept is applied to ICE vehicles. In ICE vehicles,

electrical energy required for auxiliary systems is typically generated by an engine-driven alternator. The alternator increases the engine's mechanical load, resulting in additional fuel consumption and emissions. A VIPV system can offset part of this load by providing clean electrical energy, thereby reducing fuel usage and its associated emissions. Referring to the alternator, the emissions saved can be estimated using the following equation [52–54]:

$$Em_{ICE} = W \cdot \frac{V_{Fuel} \cdot C_{Fuel}}{\eta_{Alt}} \quad (24)$$

where V_{Fuel} l/kWh is the fuel consumption to energy content ratio, η_{Alt} is the efficiency of the alternator, C_{Fuel} gCO_2/l is the CO_2 conversion factor of the fuel, and W is the energy generated by VIPV. In the previous section, the energy generated by VIPV (W) over different time steps, particularly over the course of one year for the electric minibus, was calculated. However, to ensure a fair comparison under identical conditions of solar irradiation and module area, it is assumed that the energy production from VIPV is the same across all vehicle types: electric, petrol, and diesel. For petrol and diesel fuels, the values of V_{Fuel} and C_{Fuel} were considered as 0.264 l/kWh and 2330 gCO_2/l, and 0.220 l/kWh and 2640 gCO_2/l, respectively [53]. Based on these assumptions and data, the potential amount of emissions saved by using VIPV technology in different ICE vehicle types can be estimated and is presented in Figure 17.

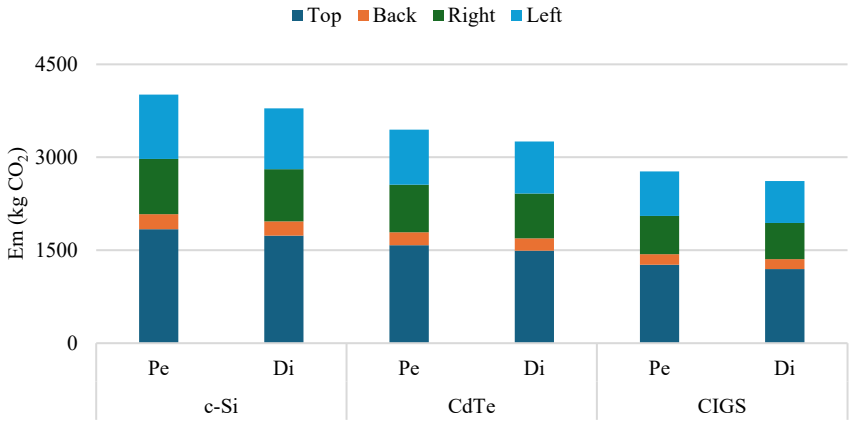

Figure 17. Emission savings achieved by using VIPV for diesel and petrol minibuses.

In this context, sustainability considerations can also be integrated by assessing how the VIPV concept may contribute to the green transition. Unlike ICE vehicles, which emit greenhouses gasses (measured in $kgCO_2eq$) directly from their tailpipes during operation, EVs produce no direct CO_2 emissions. This can represent a significant step toward sustainability if it is ensured that in the $kgCO_2eq$ generated by the production of battery and electronic components of EV is not too high. However further life cycle assessment (LCA) studies are necessary to evaluate the carbon footprint of different VIPV combinations along their life cycle that is the reason why in this study we focus our attention on the use phase as first. Another important component to consider is the electricity used to charge EVs. It is often sourced from the power grid, which may still partially depend on fossil fuels, thereby indirectly contributing to CO_2 emissions. The emissions saved by using VIPV in EVs can be estimated using the following equation [26]:

$$Em_{EV} = W \cdot Em_{Grid} \quad (25)$$

where Em_{Grid} gCO_2eq/kWh is the grid emission intensity. Since the simulation model used Typical Meteorological Year (TMY) data corresponding to the period from 2005 to 2018 in Palermo, the evaluation of grid emissions was based on this timeframe. During these years, the grid's emission intensity in Italy declined, reflecting a transition toward cleaner energy sources. For example, while the grid emission factor was approximately 0.487 $kgCO_2eq/kWh$ in 2005, it decreased to about 297 gCO_2eq/kWh in 2018 [55]. The variations in emissions saved by using VIPV technology in the electric minibus are presented in Figure 18.

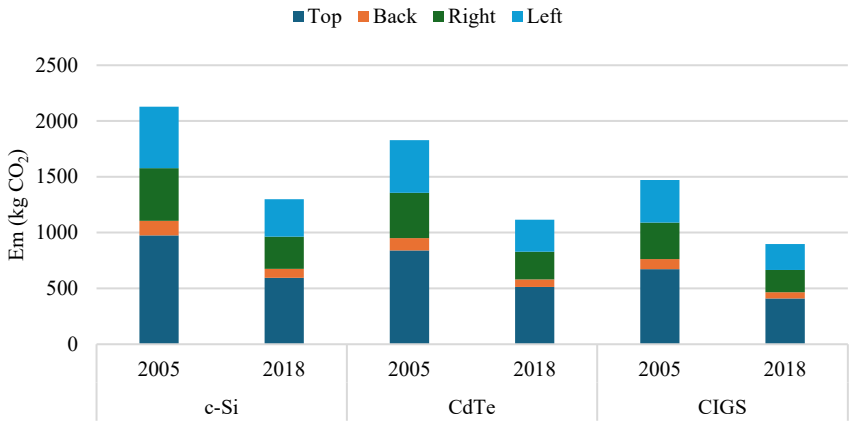

Figure 18. Emission savings achieved by using VIPV for electric minibus.

As many countries transition toward renewable energy sources, the carbon intensity of electricity generation is gradually decreasing. This shift directly affects the environmental benefit of substituting grid electricity with solar energy, such as through VIPV systems. However, the impact of this substitution varies significantly depending on the country's energy mix. In some European countries, where the electricity grid already has a low emission intensity, the environmental advantage of adding solar modules may be limited. In contrast, countries with grids that rely heavily on fossil fuels can benefit more from integrating renewable sources [56]. For instance, Iran's share of renewable energy in its electricity mix has been relatively low, peaking at around 9.5% [57]. The country's grid emission factor in 2022 was approximately 0.494 $kgCO_2eq/kWh$ [58]. In China, although a downward trend is expected, the grid emissions by 2030 are still projected to remain relatively high, in the range of 0.629–0.736 $kgCO_2eq/kWh$ [59]. As for Italy, while exact national projections for the 2030 grid emission factor are not available, individual energy companies have set their own targets. A2A aims to reduce its direct emissions by 46% compared to 2017 levels, targeting an emission factor of 0.230 $kgCO_2eq/kWh$ by 2030 [60]. This goal is supported by the expansion of renewable capacity (at least 1.6 *GW*), optimization of combined-cycle gas turbines, and a complete phase-out of coal and heavy oil. Similarly, Enel has committed to reducing its direct emissions to 0.082 $kgCO_2eq/kWh$ by 2030, as approved by the Science Based Targets initiative (SBTi) [61]. Although these companies' targets do not directly represent national grid emissions, they reflect the influence of energy mix diversification and sector-specific contributions to decarbonization. Overall, the emissions associated with electricity use are highly dependent on each country's energy mix [7,56]. Based on the results shown in Figure 18, which illustrate the emission savings from using VIPV systems between 2005 and 2018, these savings are expected to decrease by 2030.

All the values mentioned for EVs and ICE vehicles refer to avoided emissions, which are based solely on energy consumption during driving. However, the net reduction in emissions from using a VIPV system is calculated as the difference between the emissions avoided and the emissions associated with the PV system itself [62]. While PV systems do

not produce direct emissions during operation, their manufacturing, installation, and end-of-life processes do contribute to environmental impacts. To evaluate the real sustainability benefit, an LCA analysis is needed [63,64]. For example, an LCA analysis of a light electric utility vehicle in Cologne, Germany, considered emissions associated with raw material extraction, solar cell and module manufacturing, inverter and structure production, and system installation and operation, focusing on the global warming potential (GWP) and using 1 kWh of onboard PV electricity generation as the functional unit [7]. It was found that the emission factor of the VIPV electricity was 0.357 $kgCO_2eq/kWh$, while the average grid electricity had an emission factor of 0.435 $kgCO_2eq/kWh$. However, the benefit of VIPV was highly sensitive to shading and system lifetime. When the shading factor increased from 30% to 40%, the emission factor of the PV system exceeded that of the grid, resulting in no environmental gain. The same study showed that extending the system's operational lifetime from 8 to 12 years reduced the emission factor by about 0.221 $kgCO_2eq/kWh$. Another study assessed the solar energy potential of parking spaces in Berlin, incorporating data on shading from trees and buildings using digital surface models and weather-based solar simulations [65]. The findings indicated that VIPV systems could increase daily driving range by 7 to 14 km, amounting to a median annual gain of 2527 km. The study concluded that, based on the assumptions of Kanz et al. [7], the average shading losses for typical parking spaces exceeded 50%, which meant that VIPV systems, in those locations, were less sustainable than conventional grid-based charging. Another study conducted a cradle-to-gate life cycle assessment to estimate the greenhouse gas emissions associated with VIPV systems [66]. This assessment covered the entire production process, from raw material extraction to the final assembly of the solar modules and accounted for the carbon intensity of the electricity used both at the manufacturing sites and in the countries where the vehicles are operated. They applied their assessment framework to a specific case study in which monocrystalline silicon was extracted and refined in China, while the modules were assembled in the Netherlands. This process resulted in approximately 0.118 $kgCO_2eq$ per square meter of solar module. The findings suggest that electric vehicles equipped with integrated PV systems are generally more environmentally beneficial in countries with high solar irradiation. However, in regions where the electricity grid is already low in carbon emissions, the additional emissions from manufacturing the VIPV system may not be justified. In such cases, a longer vehicle lifespan would be required to achieve a net reduction in emissions.

Generally, various case studies assume that the lifetime of VIPV systems ranges between 8 and 15 years [8]. Most of the environmental impact associated with VIPV systems occurs during the manufacturing phase. Therefore, longer operational lifetimes help offset this impact more effectively over time [63]. For this reason, using solar parking, which refers to fixed photovoltaic systems installed in parking areas, is sometimes considered more sustainable than VIPV systems [56]. One reason is that residential and fixed PV systems typically have longer lifespans, often ranging from 25 to 35 years. For example, using the same PV technologies considered in this study, including monocrystalline silicon, multicrystalline silicon, CIGS, and CdTe, and assuming a service life of 30 years for PV modules and 15 years for inverters, the associated emissions can be approximately 0.036, 0.044, 0.036, and 0.025 $kgCO_2eq/kWh$, respectively [67]. However, as transport is responsible for around 30% of energy-related greenhouse gas emissions in the EU [68], developing PV modules specifically tailored for VIPV applications can play a key role in supporting the rapid growth of these technologies in the near future.

Although a full life cycle assessment is not the main objective of this paper, incorporating the discussed sustainability aspects into the analysis allows for a better understanding of the broader impact of VIPV systems. The examples provided highlight how environmen-

tal performance is influenced by contextual factors such as shading, local climate, vehicle usage patterns, and system lifetime. As a result, in some cases, the integration of a VIPV system may not lead to a net sustainability benefit. These findings show that while VIPV can offer significant sustainability advantages under favorable conditions, it may not always be the most effective solution. For example, in some countries like Sweden, emissions may increase by up to 15% instead of decreasing. However, according to previous studies [66,69], in several European countries such as Italy, Spain, and Portugal, the potential greenhouse gas (GHG) reduction from using VIPV systems can reach, or even exceed, 40%. In the specific case study presented in this paper, the comparison between internal combustion engine vehicles and electric vehicles shows that the amount of emissions avoided by using VIPV is significantly higher for internal combustion engine vehicles. When these avoided emissions are evaluated alongside the emissions produced during the manufacturing and lifecycle of the photovoltaic system, the results can be more favorable. This is especially true in locations such as the UNIPA campus, where high solar irradiance and minimal shading create ideal conditions for solar energy generation.

5. Conclusions

This study presents a structured and flexible simulation framework for VIPV systems. The proposed model chain, comprising optical, thermal, and electrical models, offers a simulation-based approach using real-world driving data instead of relying solely on experimental setups. This approach not only reduces the need for costly and often case-specific testing but also improves scalability and applicability across various vehicle types and operational conditions.

Real-time data were collected using only a smartphone, enabling precise irradiance modeling without the need for complex and expensive instrumentation. This makes the method valuable for widespread feasibility studies and early-stage assessments of VIPV systems. Furthermore, while the framework incorporates methodologies originally developed for fixed PV systems, these were carefully modified for moving vehicles, considering the dynamic nature of vehicle motion, including discrete positioning in the optical model and wind-related effects and thermal inertia, in the thermal model.

To support broader use and future development, an open-source simulation tool, referred to as 'VIPVLIB', was developed based on the proposed methodology and using PVLIB functions. This tool is made publicly available to assist researchers working on VIPV-related topics.

Experimental validation was carried out through a case study using a campus minibus operating at the University of Palermo. The full model chain was applied under real driving conditions, and its results were analyzed from multiple perspectives. Quantitatively, the total yearly energy yield reached approximately 4.3 MWh/Year for crystalline-silicon, 3.7 MWh/Year for CdTe, and 3.1 MWh/Year for CIGS. Under hourly operation, the generated solar energy was sufficient to fully meet the daily demand during summer months, whereas under continuous operation it supplied up to 60% of total consumption. The corresponding CO_2-emission reduction ranged from about 3.5 ton/Year for internal-combustion vehicles to around 2 ton/Year for electric ones. Additionally, one of the investigations focused on the effect of time resolution in simulations. While top surfaces exhibited negligible error across various time intervals, substantial deviations were observed for more dynamic side and rear surfaces, highlighting the importance of high temporal resolution for accuracy, particularly in mobile PV applications.

Additionally, the study analyzed the impact of driving scenarios, seasonal irradiance variation, PV technology selection, and passenger load on energy consumption. Results revealed that under optimal summer conditions, the VIPV system could fully meet the

hourly energy demand of the vehicle. However, when considering continuous operation, energy autonomy was achievable for only a limited period each year, emphasizing the importance of operational context in evaluating system feasibility.

The research also explored broader sustainability aspects, comparing different vehicle types, including electric and internal combustion engine vehicles, and assessing the potential emission reductions enabled by VIPV integration. Although a detailed LCA was beyond the scope of this work, the study draws on existing literature to contextualize the environmental impact of VIPV, highlighting how operational lifetime and grid cleanliness influence overall sustainability outcomes. Additionally, this research addresses some limitations of previous studies in LCA, which often focus solely on integrating PV systems into vehicle roofs, overlooking both the influence of vehicle dynamics and the potential contributions of other surfaces. By integrating these overlooked factors, using our proposed framework provides a more complete and realistic approach to evaluating sustainability in VIPV systems and lays the foundation for future advancements in the field.

Future research should focus on extending the model to other climatic regions, integrating real-time, high-frequency meteorological and shading data, and coupling the VIPV framework with advanced traffic or drive-cycle models as well as real energy-consumption datasets. Incorporating battery storage, inverter behavior, and more detailed life-cycle assessment will further strengthen its applicability for full-vehicle energy and environmental evaluations.

Author Contributions: Conceptualization, M.C.B. and G.A.; methodology, H.S., M.C.B. and G.A.; software, H.S.; validation, H.S., P.R. and F.V.; investigation, H.S.; resources, G.A., M.C.B., M.T. and F.V.; data curation, H.S., F.V. and P.R.; writing—original draft preparation, H.S., M.C.B., G.A. and M.T.; writing—review and editing, H.S., G.A., M.C.B., M.T. and S.L.; supervision, M.T., P.R. and F.V.; project administration, G.A. and M.C.B.; funding acquisition, H.S., G.A., M.C.B. and S.L. All authors have read and agreed to the published version of the manuscript.

Funding: The PhD work of Hamid Samadi contributing to this research is supported by the Italian National PhD in Photovoltaics—Curriculum: Design and Integration. This work was funded by the Portuguese Fundação para a Ciência e a Tecnologia (FCT) I.P./MCTES through national funds (PIDDAC)—UIDB/50019/2020 (https://doi.org/10.54499/UIDB/50019/2020), UIDP/50019/2020 (https://doi.org/10.54499/UIDP/50019/2020), LA/P/0068/2020 (https://doi.org/10.54499/LA/P/0068/2020), and IDL research grant UI/BD/151496/2021. This work was also financed by the European Union—NextGenerationEU (National Sustainable Mobility Center CN00000023, Italian Ministry of University and Research Decree n. 1033—17 June 2022, Spoke 12). Silvia Licciardi were supported by the following project: "Network 4 Energy Sustainable Transition—NEST", code PE0000021, CUP B73C22001280006, Spoke 7, funded under the National Recovery and Resilience Plan (NRRP), Mission 4, by the European Union—NextGenerationEU.

Data Availability Statement: The code for this study is available at: https://github.com/hamidsmd/VIPVLIB (accessed on 12 September 2025).

Conflicts of Interest: The authors declare no conflict of interest.

Glossary

List of Symbols and Parameters:

A_{PV}	Effective PV area (m^2)	$NOCT$	Nominal Operating Cell Temperature (°C)
$A_{Vehicle}$	Available geometric surface area of the vehicle (m^2)	P_{PV}	Power output of the PV system (W)
A_f	Frontal area (m^2)	P_{tot}	Total power consumption (W)
AM	Air mass	T_{module}	PV module temperature (°C)
C_{Fuel}	CO_2 conversion factor of the fuel (gCO_2/l)	T_a	Air temperature (°C)
c_d	Air drag coefficient	T_{ref}	Reference temperature (°C)
c_{rr}	Rolling resistance coefficient	U_0	Constant heat transfer component ($W/m^2°C$)
CF	Curvature factor	U_1	Convective heat transfer component ($W/m^3s°C$)
DHI	Diffuse horizontal irradiance (W/m^2)	V	Vehicle speed (m/s)
DNI	Direct normal irradiance (W/m^2)	V_{Fuel}	Fuel consumption to energy content ratio (l/kWh)
doy	Day of year	W	Energy generation (kWh)
E_a	Extraterrestrial normal irradiance (W/m^2)	WS	Wind speed (m/s)
E_{tot}	Total energy consumption (Wh)		
Em_{Grid}	Grid emission intensity (gCO_2eq/kWh)		
F_1	Circumsolar component		
F_2	Horizon brightness factor		Greek Symbols
F_a	Aerodynamic drag force (N)	α	PV coverage ratio
F_i	Inertial force (N)	α_S	solar elevation angle (°)
F_r	Rolling resistance force (N)	β	Surface tilt angle (°)
F_s	Gravitational force (N)	η_{Co}	Power converter efficiency
F_t	Total force (N)	η_{PV}	PV module efficiency
G	Incident solar irradiance (W/m^2)	$\eta_{Shading}$	Shading efficiency
G_b	Direct (beam) irradiance (W/m^2)	θ_Z	Solar zenith angle (°)
G_d	Diffuse irradiance (W/m^2)	γ	Surface azimuth angle (°)
G_r	Reflected irradiance (W/m^2)	γ_S	Solar azimuth angle (°)
h_{Roof}	Height of the vehicle roof (m)	Δ	sky's brightness
k	Temperature coefficient (%/°C)	ε	sky's clearness
M	Total mass (kg)	ρ	Air density (kg/m^3)

References

1. Yamaguchi, M.; Masuda, T.; Nakado, T.; Yamada, K.; Okumura, K.; Satou, A.; Ota, Y.; Araki, K.; Nishioka, K.; Kojima, N.; et al. Analysis for Expansion of Driving Distance and CO_2 Emission Reduction of Photovoltaic-Powered Vehicles. *IEEE J. Photovolt.* **2023**, *13*, 343–348. [CrossRef]
2. Ala, G.; Di Filippo, G.; Viola, F.; Giglia, G.; Imburgia, A.; Romano, P.; Castiglia, V.; Pellitteri, F.; Schettino, G.; Miceli, R. Different Scenarios of Electric Mobility: Current Situation and Possible Future Developments of Fuel Cell Vehicles in Italy. *Sustainability* **2020**, *12*, 564. [CrossRef]
3. Ala, G.; Colak, I.; Di Filippo, G.; Miceli, R.; Romano, P.; Silva, C.; Valtchev, S.; Viola, F. Electric Mobility in Portugal: Current Situation and Forecasts for Fuel Cell Vehicles. *Energies* **2021**, *14*, 7945. [CrossRef]
4. Almonacid, G.; Muñoz, F.J.; de la Casa, J.; Aguilar, J.D. Integration of PV systems on health emergency vehicles. The FIVE project. *Prog. Photovolt. Res. Appl.* **2004**, *12*, 609–621. [CrossRef]
5. Kronthaler, L.; Maturi, L.; Moser, D.; Alberti, L. Vehicle-integrated Photovoltaic (ViPV) systems: Energy production, Diesel Equivalent, Payback Time; an assessment screening for trucks and busses. In *Proceedings of the 2014 Ninth International Conference on Ecological Vehicles and Renewable Energies (EVER)*; Monte-Carlo, Monaco, 25–27 March 2014, IEEE: New York, NY, USA, 2014; pp. 1–8. [CrossRef]
6. Brito, M.C.; Santos, T.; Moura, F.; Pera, D.; Rocha, J. Urban solar potential for vehicle integrated photovoltaics. *Transp. Res. Part D Transp. Environ.* **2021**, *94*, 102810. [CrossRef]
7. Kanz, O.; Reinders, A.; May, J.; Ding, K. Environmental Impacts of Integrated Photovoltaic Modules in Light Utility Electric Vehicles. *Energies* **2020**, *13*, 5120. [CrossRef]
8. Karoui, F.; Chambion, B.; Claudon, F.; Commault, B. Integrated Photovoltaics Potential for Passenger Cars: A Focus on the Sensitivity to Electrical Architecture Losses. *Appl. Sci.* **2023**, *13*, 8373. [CrossRef]

9. Karoui, F.; Claudon, F.; Chambion, B.; Catellani, S.; Commault, B. Estimation of integrated photovoltaics potential for solar city bus in different climate conditions in Europe. *J. Phys. Conf. Ser.* **2023**, *2454*, 012007. [CrossRef]
10. Yamaguchi, M.; Masuda, T.; Araki, K.; Sato, D.; Lee, K.; Kojima, N.; Takamoto, T.; Okumura, K.; Satou, A.; Yamada, K.; et al. Development of high-efficiency and low-cost solar cells for PV-powered vehicles application. *Prog. Photovolt. Res. Appl.* **2020**, *29*, 684–693. [CrossRef]
11. Martins, A.C.; Chapuis, V.; Virtuani, A.; Ballif, C. Robust Glass-Free Lightweight Photovoltaic Modules with Improved Resistance to Mechanical Loads and Impact. *IEEE J. Photovolt.* **2019**, *9*, 245–251. [CrossRef]
12. Kim, S.; Holz, M.; Park, S.; Yoon, Y.; Cho, E.; Yi, J. Future Options for Lightweight Photovoltaic Modules in Electrical Passenger Cars. *Sustainability* **2021**, *13*, 2532. [CrossRef]
13. HSamadi, H.; Ala, G.; Brano, V.L.; Romano, P.; Viola, F. Investigation of Effective Factors on Vehicles Integrated Photovoltaic (VIPV) Performance: A Review. *World Electr. Veh. J.* **2023**, *14*, 154. [CrossRef]
14. Peibst, R.; Fischer, H.; Brunner, M.; Schiessl, A.; Wöhe, S.; Wecker, R.; Haase, F.; Schulte-Huxel, H.; Blankemeyer, S.; Köntges, M.; et al. Demonstration of Feeding Vehicle-Integrated Photovoltaic-Converted Energy into the High-Voltage On-Board Network of Practical Light Commercial Vehicles for Range Extension. *Sol. RRL* **2022**, *6*, 2100516. [CrossRef]
15. Ota, Y.; Masuda, T.; Araki, K.; Yamaguchi, M. Curve-Correction Factor for Characterization of the Output of a Three-Dimensional Curved Photovoltaic Module on a Car Roof. *Coatings* **2018**, *8*, 432. [CrossRef]
16. Wetzel, G.; Salomon, L.; Krügener, J.; Bredemeier, D.; Peibst, R. High time resolution measurement of solar irradiance onto driving car body for vehicle integrated photovoltaics. *Prog. Photovolt. Res. Appl.* **2022**, *30*, 543–551. [CrossRef]
17. Araki, K.; Ota, Y.; Nishioka, K. Testing and rating of vehicle-integrated photovoltaics: Scientific background. *Sol. Energy Mater. Sol. Cells* **2025**, *280*, 113241. [CrossRef]
18. Araki, K.; Ota, Y.; Nagaoka, A.; Nishioka, K. 3D Solar Irradiance Model for Non-Uniform Shading Environments Using Shading (Aperture) Matrix Enhanced by Local Coordinate System. *Energies* **2023**, *16*, 4414. [CrossRef]
19. Park, C.; Park, H.; Jeon, H.; Choi, K.; Suh, J. Evaluation and Validation of Photovoltaic Potential Based on Time and Pathway of Solar-Powered Electric Vehicle. *Appl. Sci.* **2023**, *13*, 1025. [CrossRef]
20. Araki, K.; Ota, Y.; Maeda, A.; Kumano, M.; Nishioka, K. Solar Electric Vehicles as Energy Sources in Disaster Zones: Physical and Social Factors. *Energies* **2023**, *16*, 3580. [CrossRef]
21. Samadi, H.; Ala, G.; Brito, M.C.; Marcon, G.; Romano, P.; Viola, F. Vehicle-Integrated Photovoltaic (VIPV) for Sustainable Airports: A Flexible Framework for Performance Assessment. *Sustainability* **2025**, *17*, 9246. [CrossRef]
22. Oh, M.; Kim, S.-M.; Park, H.-D. Estimation of photovoltaic potential of solar bus in an urban area: Case study in Gwanak, Seoul, Korea. *Renew Energy* **2020**, *160*, 1335–1348. [CrossRef]
23. Kim, H.; Ku, J.; Kim, S.-M.; Park, H.-D. A new GIS-based algorithm to estimate photovoltaic potential of solar train: Case study in Gyeongbu line, Korea. *Renew Energy* **2022**, *190*, 713–729. [CrossRef]
24. Kutter, C.; Alanis, L.E.; Neuhaus, D.H.; Heinrich, M. Yield Potential of Vehicle Integrated Photovoltaics on Commercial Trucks and Vans. 2021. Available online: https://www.researchgate.net/publication/355126708 (accessed on 8 November 2025).
25. Abdelhamid, M.; Pilla, S.; Singh, R.; Haque, I.; Filipi, Z. A comprehensive optimized model for on-board solar pho-tovoltaic system for plug-in electric vehicles: Energy and economic impacts. *Int. J. Energy Res.* **2016**, *40*, 1489–1508. [CrossRef]
26. Samadi, H.; Ala, G.; Imburgia, A.; Licciardi, S.; Romano, P.; Viola, F. Evaluating the Role of Vehicle-Integrated Pho-tovoltaic (VIPV) Systems in a Disaster Context. *World Electr. Veh. J.* **2025**, *16*, 190. [CrossRef]
27. Samadi, H.; Hosseini, M.; Ranjbar, A.; Pahamli, Y. Thermohydraulic performance of new minichannel heat sink with grooved barriers. *Int. Commun. Heat Mass Transf.* **2023**, *144*, 106753. [CrossRef]
28. Fard, M.S.; Rahimi, M.; Pahamli, Y.; Samadi, H.; Bahrampoury, R. Cooling performance of sliver solar cells in low concentration PV system with ribbed-groove mini-channel heat sink. *Int. J. Therm. Sci.* **2024**, *200*, 108955. [CrossRef]
29. Hayakawa, Y.; Sato, D.; Yamada, N. Measurement of the Convective Heat Transfer Coefficient and Temperature of Vehicle-Integrated Photovoltaic Modules. *Energies* **2022**, *15*, 4818. [CrossRef]
30. Yamaguchi, M.; Masuda, T.; Araki, K.; Ota, Y.; Nishioka, K.; Takamoto, T.; Thiel, C.; Tsakalidis, A.; Jaeger-Waldau, A.; Okumura, K.; et al. Analysis of temperature coefficients and their effect on efficiency of solar cell modules for pho-tovoltaics-powered vehicles. *J. Phys. D Appl. Phys.* **2021**, *54*, 504002. [CrossRef]
31. Yamaguchi, M.; Ota, Y.; Masuda, T.; Thiel, C.; Tsakalidis, A.; Jaeger-Waldau, A.; Araki, K.; Nishioka, K.; Takamoto, T.; Nakado, T.; et al. Analysis for Effects of Temperature Rise of PV Modules upon Driving Distance of Vehicle Inte-grated Photovoltaic Electric Vehicles. *Energy Power Eng.* **2024**, *16*, 131–150. [CrossRef]
32. Golubev, T.; Lunt, R.R. Evaluating the Electricity Production of Electric Vehicle-Integrated Photovoltaics via a Coupled Modeling Approach. In Proceedings of the 2021 IEEE 48th Photovoltaic Specialists Conference (PVSC), Fort Lauderdale, FL, USA, 20–25 June 2021; IEEE: New York, NY, USA, 2021; pp. 0155–0159. [CrossRef]

33. Bharti, R.; Kuitche, J.; TamizhMani, M.G. Nominal Operating Cell Temperature (NOCT): Effects of module size, loading and solar spectrum. In Proceedings of the 2009 34th IEEE Photovoltaic Specialists Conference (PVSC), Philadelphia, PA, USA, 7–12 June 2009; IEEE: New York, NY, USA, 2009; pp. 001657–001662. [CrossRef]
34. Faiman, D. Assessing the outdoor operating temperature of photovoltaic modules. *Prog. Photovolt. Res. Appl.* **2008**, *16*, 307–315. [CrossRef]
35. Patel, N.; Pieters, B.E.; Bittkau, K.; Sovetkin, E.; Ding, K.; Reinders, A. Assessing the accuracy of two steady-state temperature models for onboard passenger vehicle photovoltaics applications. *Prog. Photovolt. Res. Appl.* **2024**, *32*, 790–798. [CrossRef]
36. Mallon, K.R.; Assadian, F.; Fu, B. Analysis of On-Board Photovoltaics for a Battery Electric Bus and Their Impact on Battery Lifespan. *Energies* **2017**, *10*, 943. [CrossRef]
37. Perez, R.; Ineichen, P.; Seals, R.; Michalsky, J.; Stewart, R. Modeling daylight availability and irradiance components from direct and global irradiance. *Sol. Energy* **1990**, *44*, 271–289. [CrossRef]
38. King, D.; Kratochvil, J.; Boyson, W. Measuring solar spectral and angle-of-incidence effects on photovoltaic modules and solar irradiance sensors. In Proceedings of the Conference Record of the Twenty Sixth IEEE Photovoltaic Specialists Conference-1997, Anaheim, CA, USA, 29 September–3 October 1997; IEEE: New York, NY, USA; pp. 1113–1116. [CrossRef]
39. European Commission. Photovoltaic Geographical Information System. Available online: https://re.jrc.ec.europa.eu/pvg_tools/en/ (accessed on 11 April 2024).
40. Samadi, H.; Ala, G.; Brano, V.L.; Romano, P.; Viola, F.; Miceli, R. Potential and Methods of Integrating Solar Cells into Vehicles. In Proceedings of the 2023 International Conference on Clean Electrical Power (ICCEP), Sicily, Italy, 27–29 June 2023; IEEE: New York, NY, USA, 2023; pp. 715–720. [CrossRef]
41. Duffie, J.A.; Beckman, W.A. *Solar Engineering of Thermal Processes*; Wiley: New York, NY, USA, 2013. [CrossRef]
42. Rakovec, J.; Zakšek, K. On the proper analytical expression for the sky-view factor and the diffuse irradiation of a slope for an isotropic sky. *Renew Energy* **2012**, *37*, 440–444. [CrossRef]
43. Ota, Y.; Araki, K.; Nagaoka, A.; Nishioka, K. Facilitating vehicle-integrated photovoltaics by considering the radius of curvature of the roof surface for solar cell coverage. *Clean. Eng. Technol.* **2022**, *7*, 100446. [CrossRef]
44. Kasten, F.; Young, A.T. Revised optical air mass tables and approximation formula. *Appl. Opt.* **1989**, *28*, 4735–4738. [CrossRef]
45. Anderson, K.S.; Hansen, C.W.; Holmgren, W.F.; Jensen, A.R.; Mikofski, M.A.; Driesse, A. Pvlib python: 2023 project update. *J. Open Source Softw.* **2023**, *8*, 5994. [CrossRef]
46. Thiel, C.; Amillo, A.G.; Tansini, A.; Tsakalidis, A.; Fontaras, G.; Dunlop, E.; Taylor, N.; Jäger-Waldau, A.; Araki, K.; Nishioka, K.; et al. Impact of climatic conditions on prospects for integrated photovoltaics in electric vehicles. *Renew. Sustain. Energy Rev.* **2022**, *158*, 112109. [CrossRef]
47. Kumar, N.M.; Ghosh, A.; Chopra, S.S. Power Resilience Enhancement of a Residential Electricity User Using Photovoltaics and a Battery Energy Storage System under Uncertainty Conditions. *Energies* **2020**, *13*, 4193. [CrossRef]
48. Campagna, N.; Castiglia, V.; Gennaro, F.; Messina, A.A.; Miceli, R. Fuel Cell-Based Inductive Power Transfer System for Supercapacitor Constant Current Charging. *Energies* **2024**, *17*, 3575. [CrossRef]
49. Karsan, B.M. Electric Minibus with Zero Emissions, Karsan e-JEST. Available online: https://www.karsan.com/en/e-jest-highlights#e-jest-specs (accessed on 16 September 2024).
50. Fraunhofer Institute for Solar Energy Systems. Photovoltaics Report. 2024. Available online: https://www.ise.fraunhofer.de/content/dam/ise/de/documents/publications/studies/Photovoltaics-Report.pdf (accessed on 18 November 2024).
51. Kumar, N.M.; Chopra, S.S.; Malvoni, M.; Elavarasan, R.M.; Das, N. Solar Cell Technology Selection for a PV Leaf Based on Energy and Sustainability Indicators—A Case of a Multilayered Solar Photovoltaic Tree. *Energies* **2020**, *13*, 6439. [CrossRef]
52. European Commission. *Technical Guidelines for the Preparation of Applications for the Approval of Innovative Technologies Pursuant to Regulation (EC) No 443/2009 and Regulation (EU) No 510/2011*; European Commission: Brussels, Belgium, 2015.
53. Lodi, C.; Seitsonen, A.; Paffumi, E.; De Gennaro, M.; Huld, T.; Malfettani, S. Reducing CO_2 emissions of conventional fuel cars by vehicle photovoltaic roofs. *Transp. Res. D Transp. Environ.* **2018**, *59*, 313–324. [CrossRef]
54. Lodi, C.; Gil-Sayas, S.; Currò, D.; Serra, S.; Drossinos, Y. Full-battery effect during on-board solar charging of con-ventional vehicles. *Transp. Res. D Transp. Environ.* **2021**, *96*, 102862. [CrossRef]
55. Istituto Superiore per la Protezione e la Ricerca Ambientale. *Efficiency and Decarbonization Indicators in Italy and in the Biggest European Countries, Edition 2023*; Istituto Superiore per la Protezione e la Ricerca Ambientale: Rome, Italy, 2023.
56. Miceli, R.; Viola, F. Designing a Sustainable University Recharge Area for Electric Vehicles: Technical and Economic Analysis. *Energies* **2017**, *10*, 1604. [CrossRef]
57. Peyvandi, M.; Hajinezhad, A.; Moosavian, S.F. Investigating the intensity of GHG emissions from electricity pro-duction in Iran using renewable sources. *Results Eng.* **2023**, *17*, 100819. [CrossRef]
58. Global Electricity Review 2023/Country and Region Deep Dives. Available online: https://ember-energy.org/latest-insights/global-electricity-review-2023/country-and-region-deep-dives/#iran (accessed on 5 July 2025).

59. Zhang, X.; Xu, K. Statistical data-based prediction of carbon dioxide emission factors of China's power generation at carbon peak in 2030. *Case Stud. Therm. Eng.* **2023**, *51*, 103633. [CrossRef]
60. A2A Will Reduce Greenhouse Gas Emissions by 46% by 2030. Available online: https://www.gruppoa2a.it/en/media/press-releases/a2a-will-reduce-greenhouse-gas-emissions-46-2030 (accessed on 25 July 2025).
61. Enel Boosts Its 2030 Greenhouse Gas Emission Reduction Target to 80% from 70%, SBTi-Certified. Available online: https://corporate.enel.it/content/dam/enel-common/press/en/2020-October/Enel%20SBTI%20upgraded.pdf (accessed on 7 June 2025).
62. New Energy and Industrial Technology Development Organization. *PV-Powered Vehicle Strategy Committee Interim Report*; New Energy and Industrial Technology Development Organization: Kanagawa, Japan, 2018.
63. Kanz, O.; Reinders, A.; May, J.; Ding, K. Environmental Impacts of Integrated Photovoltaic Modules in Light Utility Vehicles. In *Photovoltaic Solar Energy*; Wiley: New York, NY, USA, 2024; pp. 567–577. [CrossRef]
64. Traverso, M.; Asdrubali, F.; Francia, A.; Finkbeiner, M. Towards life cycle sustainability assessment: An implemen-tation to photovoltaic modules. *Int. J. Life Cycle Assess.* **2012**, *17*, 1068–1079. [CrossRef]
65. Hoth, P.; Heide, L.; Grahle, A.; Göhlich, D. Vehicle-Integrated Photovoltaics—A Case Study for Berlin. *World Electr. Veh. J.* **2024**, *15*, 113. [CrossRef]
66. Clemente, M.; Van Sundert, L.; Salazar, M.; Hofman, T. A Framework to Estimate Life Cycle Emissions for Vehi-cle-Integrated Photovoltaic Systems. In Proceedings of the 2024 IEEE Vehicle Power and Propulsion Conference (VPPC), Washington, DC, USA, 7–10 October 2024; IEEE: New York, NY, USA, 2024; pp. 1–6. [CrossRef]
67. IEA Photovoltaic Power Systems Programme (PVPS). *Environmental Life Cycle Assessment of Electricity from PV Systems*; International Energy Agency (IEA): Paris, France, 2023.
68. Tous, L.; Govaert, J.; Harrison, S.; Carrière, C.; Barth, V.; Giglia, V.; Buchholz, F.; Chen, N.; Halm, A.; Faes, A.; et al. Overview of key results achieved in H2020 HighLite project helping to raise the EU PV industries' com-petitiveness. *Prog. Photovolt. Res. Appl.* **2023**, *31*, 1409–1427. [CrossRef]
69. Scarlat, N.; Prussi, M.; Padella, M. Quantification of the carbon intensity of electricity produced and used in Europe. *Appl. Energy* **2022**, *305*, 117901. [CrossRef]